ORIGINAL PAPER

Evidence for adiabatic decompression melting in the Southern Mariana Arc from high-Mg lavas and melt inclusions

Edward J. Kohut · Robert J. Stern ·
Adam J. R. Kent · Roger L. Nielsen ·
Sherman H. Bloomer · Matthew Leybourne

Abstract Unusually magnesian (Mg# ~76) basalts have been sampled from a small submarine volcano situated on the Mariana arc magmatic front. Total alkalis range from 1.7 to 1.94%, Al_2O_3 from 9.09 to 10.3% and CaO from 13.9 to 14.09%. These lavas can be classified based on mineralogy as picrite and anka-ramite. Olivine-hosted melt inclusions (MIs) have median MgO contents of 17.17–17.86 wt%, 0.35–0.5% TiO_2, 42–50% SiO_2 and 1.66–3.43% total alkalis, which suggest that the parental magmas were primitive mantle melts. Trace element concentrations for both MIs and lavas are arc-like, although more depleted than most arc lavas. Chlorine (182–334 ppm) and H_2O contents (0.11–0.64 wt%) in the MIs are consistent with the estimated median oxygen fugacities (log ΔFMQ of + 1.53–1.66) which lie at the low end of the range estimates for arc basalts and picrites (ΔFMQ = + 1 to + 3). Isotopic compositions of Sr, Nd, Hf and Pb are similar to those of other Mariana arc lavas and indicate derivation from an Indian Ocean mantle domain. The averaged magmatic temperature estimate from several geothermometers was 1,367°C at 1–1.5 GPa. We propose that high-Mg magmagenesis in this region results from the adiabatic decompression melting of relatively anhydrous but metasomatized mantle wedge. This melting is attributed to enhanced upwelling related to unusual tectonics on the over-riding plate related to a tear or other discontinuity on the subducted slab.

E. J. Kohut · A. J. R. Kent · R. L. Nielsen
Department of Geosciences, Oregon State University,
Corvallis, OR 97331, USA

R. J. Stern · M. Leybourne
Geosciences Department, University of Texas at Dallas,
Richardson, TX 75083-0688, USA

S. H. Bloomer
College of Science, Oregon State University,
Corvallis, OR 97331, USA

E. J. Kohut (✉)
Department of Geology, University of Delaware,
Newark, DE 19716, USA
e-mail: ekoh@udel.edu

Introduction

Background

The generation of melts above subduction zones is one of the most important unresolved problems for understanding the operation of the Earth system. It is especially important to understand the composition of unmodified primary magmas, as the chemistry of these melts can provide (through geothermometry, geoba-rometry and experimental reproduction) constraints on the compositional and thermal structure of sub-arc mantles (Myers and Johnston 1996; Hirschmann et al. 2000; Falloon and Danyushevsky 2000). Primary melts also provide a baseline for estimating the extent of fractionation required to generate arc and, ultimately, continental crust. The information that can be extracted from a detailed understanding of primary

melts thus provides a uniquely important perspective on magmagenesis at the convergent plate margins.

It is presumed that the subduction zone primary magmas have compositions consistent with little modified equilibrium melts of mantle peridotite and thus are magnesian, with FeO/MgO < 1. Primary magma compositions could be determined by examining samples of primitive lavas (MgO > 8 wt% and Mg#s > 70) that have suffered little modification between melt generation and eruption. Although boninites, unusual magnesian andesitic lavas, commonly erupt during the early stages in the evolution of a convergent margin or subduction zone re-initiation (Kimura et al. 2005), the occurrences of primitive arc lavas along the magmatic front of a mature arc are rare (Lee and Stern 1998; Hirschmann et al. 2000). There are, however, a few notable examples of primitive arc lavas (e.g., Tonga—Hawkins et al. 2003; New Georgia, Solomons—Scuth et al. 2003; Monzier et al. 1997; Ramsay et al. 1984; Aoba, Vanuatu—Eggins 1993; Epi, Vanuatu—Della-Pasqua and Varne 1997; southern terminus of Vanuatu arc—Monzier et al. 1997 ; Northern Tonga forearc—Danyushevsky et al. 1995; Okmok, western Aleutians—Nye and Reid 1986). Crucial data on subduction zone magmagenesis, that may be obtained from these primitive arc lavas, coupled with their relative scarcity provide compelling reasons for a detailed examination of any newly discovered example.

One mechanism for producing primitive magmas in subduction zones is via the water-poor (> 0.5%), adiabatic decompression melting more typical of mid-ocean ridge or hotspot environments rather than the hydrous flux melting classically associated with this setting. There is a growing body of evidence for this mode of magmagenesis above subduction zones (e.g., Nye and Reid 1986; Bacon et al. 1997; Sisson and Bronto 1998; Cameron et al. 2002). Because they are unusual, decompression melts could also be symptomatic of local tectonic complexities of the subduction zone under study (e.g. slab windows, slab tears or intraplate rifting).

In this paper, we present the analyses of magnesian picrite and ankaramite sampled from a previously unknown submarine volcano along the Mariana arc magmatic front. In contrast with most earlier studies of primitive arc lavas (exceptions include Sobolev and Danyushevsky 1994; Danyushevsky et al. 1995; Kamenetsky et al. 1995; Della-Pasqua and Varne 1997), we also provide data from the melt included in Fo_{88-92} phenocrysts in the picrite. Melt inclusion (MI) analyses such as these may directly sample mantle melts and circumvent possible shallow level modifications (e.g. Roedder 1979; Bacon et al. 1992; Sobolev 1996; Saal et al. 1998; Nielsen et al. 1995; Sisson and Bronto 1998; Sours-Page et al. 1999; Danyushevsky et al. 2000; Gaetani and Watson 2002; Danyushevsky et al. 2002; Kent and Elliot 2002). MIs are particularly scarce in the less abundant olivine in the ankaramite and consequently we limit our discussion of that lava to bulk compositions.

Although MI data may seem unnecessary for primitive arc lavas (Mg#s > 70), even these may have been modified between partial melting and eruption. Whole rock analyses and models derived from such data may not accurately reflect the parental components that could be obscured by minor fractionation, magma mixing, crustal contamination or crystal accumulation. In addition, micro-analysis techniques can probe MIs to reveal the amount of easily degassed components such as water in the parental melt, and this can be linked to the addition of slab-derived components. Additionally, MI may provide data that allow the P–T conditions of melting to be modeled. Experiments using high-MgO lavas with low phenocryst contents (e.g., Tatsumi 1982; Tatsumi et al. 1983, 1994; Gust and Perfit 1987; Bartels et al. 1994; Draper and Johnston 1992) produced liquids that were in equilibrium with mantle mineral assemblages, although the temperatures were ~1,290–1,360°C at significantly lower pressures (0.9–1.7 GPa) than predicted by many models of subduction zone geotherms (e.g. Myers and Johnston 1996; Peacock and Wang 1999; Davies and Stevenson 1992). It is possible that higher geothermal gradients may exist in subduction zones, as suggested by viscosity dependent models (Furukawa 1993; Van Keken et al. 2002; Peacock 2003). Studies of primitive arc lavas are thus essential for resolving this controversy.

Geological setting

The Mariana arc is the southern portion of an extended tripartite system that together with the Izu and Bonin arc are collectively referred to as the Izu Bonin–Mariana (IBM) arc system (Stern et al. 2003). This system extends over 2,800 km from the Izu Peninsula on Honshu Island, Japan, to the south of Guam. The IBM arc is a commonly cited example of an intra-oceanic arc system built on oceanic crust (e.g. Hirschmann et al. 2000; Leat and Larter 2003). The magmatic Mariana arc itself is subdivided into the Northern Seamount Province, Central Island Province and the Southern Seamount Province. Several seamount cross-chains extend from the magmatic front towards an actively spreading back-arc basin, the Marianas Trough (Bloomer et al. 1989; Stern et al. 2003). Because the IBM system is an intra-oceanic convergent margin,

contamination by continental crust and continent-derived sediment input that otherwise obscure the mantle signal is not a problem.

The lavas that are the focus of this paper were sampled from an arc-front seamount that we named Chaife, from the god of the forge in Chamorro mythology. Chaife seamount is a small volcano (possibly a parasitic cone) adjacent to the north flank of a larger volcanic edifice at the Mariana arc magmatic front, northwest of Rota (Fig. 1). These volcanoes are part of a cross-chain near 14°40′N that consist of eight or nine small volcanoes (1.3–120 km^3; mean ~ 27 km^3), which is an unusual distribution of volcanism in the Mariana arc. Mantle P-wave tomography, shallow seismicity and focal mechanisms, and the GPS results suggest that the 14°40′N cross-chain may have formed in response to a tear or other discontinuity in the subducted Pacific plate (Miller et al. 2004).

Lavas were sampled by chain-bag dredge (D14) from R/V Melville during Leg 7 of the Cook Expedition, spring 2001 (Bloomer and Stern 2001). D14 occurred at 14°39.7′N, 145°0.02′E at a depth of 1,860–2,188 m. Approximately 15 kg of vesiculated lava, Mn crust and black basaltic sand were recovered by the dredge.

Analytical methods

Detailed descriptions of the analytical methods are in Appendix I in the Electronic Supplementary Material. For whole rocks, the major elements were analyzed by activation laboratories using ICP-MS and the trace and rare earth elements were analyzed on a Perkin Elmer—Sciex Elan 6100 DRC ICP-MS at the University of Texas-Dallas. Sr, Nd and the Pb isotope data were determined using the Finnigan MAT 261 solid-source mass spectrometer at UTD and the Hf isotopes were analyzed by ICP-MS–MC at the Washington State University under the direction of Jeff Vervoort. The lavas were dated using the $^{40}Ar/^{39}Ar$ method by John Huard and Robert Duncan at the Noble Gas Mass Spectrometry laboratory at Oregon State University. Mineral and MI major element data were obtained using a Cameca SX-50 EPMA at the Oregon State University. MI trace elements were analyzed with laser ablation ICP-MS (LA–ICP-MS) in the W.M. Keck Collaboratory for Plasma Spectrometry, Oregon State University and the water contents analyses were performed with the Thermo Nicolet 670 FTIR operated by Omnic software at the University of Oregon under the direction of Paul Wallace.

Fig. 1 a Map showing the location of the Chaife Smt. Star in the Mariana arc. b Inset shows bathymetry and location dredged by the Cook 7 expedition, April 2001. Picritic and ankaramitic lavas sampled from Chaife Smt. by dredge 14 (D14). Note cross-arc chains of seamounts in the vicinity of Chaife
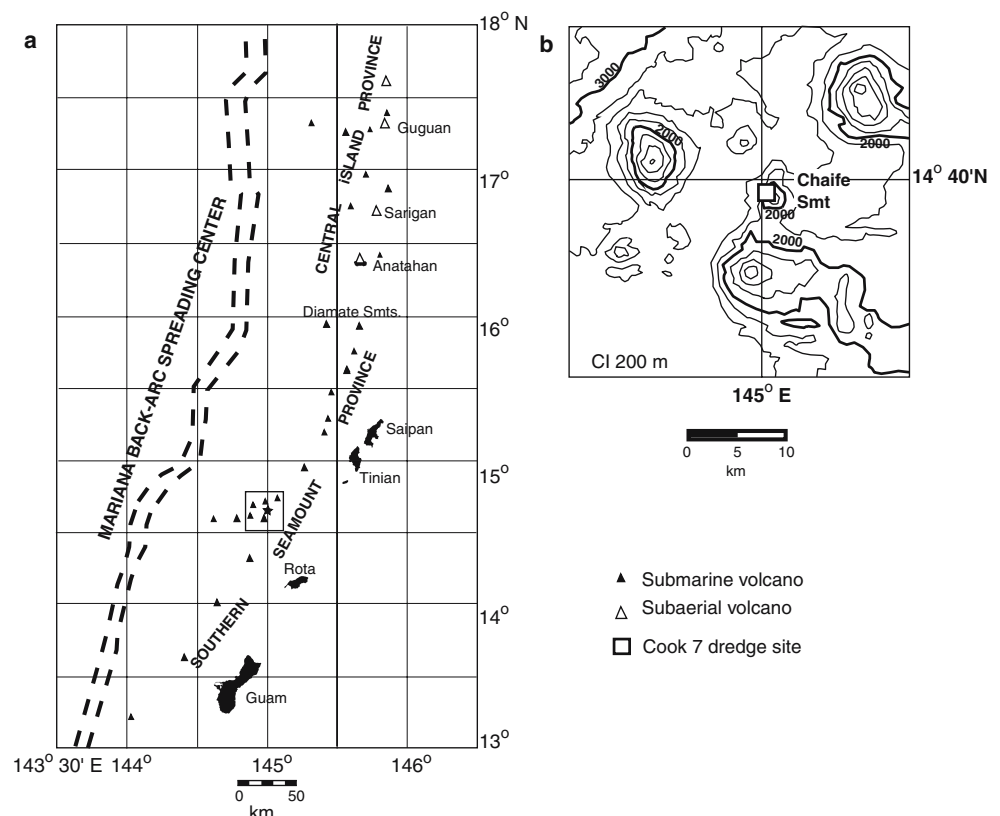
Results

Petrography and phase chemistry

Chaife lavas are classified on the basis of the mineral mode and texture as ankaramite (D14 type 1) and picrite (D14 type 4). The picrite is a medium gray vesiculated, porphyritic rock with a thin (~ 0.2 mm) veneer of Mn. Vesicles are round to lobate and ~ 0.6–2 mm in size. Rare ~ 80 mm crystal clots of olivine, pyroxene and spinel are also observed. The typical lava is 38 vol.% phenocrysts, 47 vol.% groundmass and 15 vol.% vesicles. The groundmass is vitrophyric and varies from quenched plagioclase in glass to diabasic CPX and feldspar with minor interstitial glass. Typical phenocryst assemblages are 58 % olivine, 34% CPX, 6% spinel and minor plagioclase. Both olivine and CPX are 0.3–3 mm in size and are unstrained (lacking undulatory extinction or kink bands) euhedral crystals with smooth faces, which attests to a magmatic origin. The polyhedral morphology of the phenocrysts and the scarcity of MIs suggest that crystallization mostly occurred with slow cooling, possibly near isothermal (Donaldson 1976; Faure et al. 2003; Kohut and Nielsen 2004). Spinels are more common as inclusions than as phenocrysts and both olivine and CPX commonly include spinel. A few CPX inclusions in olivine are observed. Rare (< 1 vol%) $An_{87–92}$ plagioclase phenocrysts are subhedral with albite twinning and some fritted margins. These are possibly xenocrysts. Otherwise, plagioclase occurs only as a groundmass phase. Based on these observations we determined that the crystallization history was Cr-sp → Ol + Cr-sp → Ol + +CPX → groundmass. This is similar to the crystallization sequence observed both in natural samples and in experimental run products for other arc picrites and ankaramites (Monzier et al. 1997; Ramsay et al. 1984; Eggins 1993; Della-Pasqua and Varne 1997; Green et al. 2004). Chaife lavas do not have an orthopyroxene in their crystallization sequence, which distinguishes them mineralogically from boninites (Crawford et al. 1989; Green et al. 2004).

Polycrystalline aggregates, or crystals clots, are present in the picrite, but are uncommon. These clots consist of several adjoining olivine and CPX, similar in size and morphology to the individual phenocrysts. One larger crystal clot examined is ~0.8 cm in diameter and consists of ~90% 0.8–2 mm olivine with CPX and interstitial spinel. Glass is also interstitial along some grain boundaries. In the large crystal clot, the minerals differ from the phenocrysts in that they are subhedral, and CPX are usually smaller than the olivine. Melt and spinel inclusions are not present in the olivines in this clot. In both the small and large crystal clots, olivine and CPX are unstrained.

The typical ankaramitic lava (D14-1) is more phyric than the picrite with 45% phenocrysts, 45% diabasic groundmass and 10% vesicles. The latter are generally round and are of a size ~0.05–1 mm. The smaller vesicle size relative to those in the picrite may suggest that the ankaramite erupted at a greater depth. Phenocryst assemblages are typically 65% CPX and 35% olivine. The groundmass consists of diabasic CPX and plagioclase with minor olivine and Cr-spinel. Crystal clots are absent in the ankaramite. Clinopyroxene phenocrysts are 0.5–2 mm in size and are generally larger than the olivines, which are 0.1–1 mm.

In the picrite (D14-4), olivine phenocrysts are $Fo_{84.6–93.0}$ (Table 1), CPX phenocrysts have compositions of $Wo_{44.5–47.9}$, $En_{43.8–51.7}$, $Fs_{2.9–6.2}$ and Mg#s of 88.4–92.0 (Table 2), and chromites have Cr#s (Cr/Cr + Al) of 0.60–0.77 and Mg#s $(Mg/Mg + Fe^{2+})$ of 0.59–0.93 (Table 3). The phenocrysts are largely unzoned. The olivine and CPX in crystal clots are chemically identical to the most primitive examples of these phases present as single crystals.

The olivines in the ankaramite (D14-1) are very similar to those of the picrite, with Fo contents of 88.5–92.0. The ankaramite CPX have compositions of $Wo_{43.0–46.9}$, $En_{43.8–51.5}$, $Fs_{4.4–8.6}$ and Mg#s of 84.8–92.1 (Table 2). These CPX compositions are similar to those in the picrite, with the exception of Cr which is ~0.04–0.15 wt% higher at comparable Mg#s (Table 2). Groundmass spinels are too small to effectively analyze. Comprehensive sets of mineral data are included in the Electronic Supplemental Data.

The NiO/MgO and FeO/MgO K_Ds for olivine and melt in the Chaife lavas lie both within and outside the equilibrium ranges defined by Takahashi (1978) (Fig. 2a). Many (including most hosting primary MIs) are in equilibrium with the lava. The olivines not in equilibrium with the bulk lava compositions are likely accumulated residue from a fractionated liquid. Some non-equilibrium olivines with low-CaO may be disaggregated from the source rock via high degrees of melting, as suggested by Rohrbach et al. (2005) for the New Georgia picrite olivines. However, the NiO contents of most olivines are less than 0.2 wt% in both lava types (Table 1). In contrast, abyssal peridotite olivines have 0.28–0.41 wt% NiO at $Fo_{90–91}$ (Dick 1989; Elthon et al. 1992), indicating that most Chaife olivines are unlikely to be xenocrysts from mantle peridotite. A further test of equilibrium follows that used in Tatsumi et al. (2003). A comparison of the NiO vs. Fo content for the olivines shows that many in the picrite plot along a compositional trend for olivines in

Table 1 Representative olivine analyses (cores)

	1	2	3	4	5	6	7	8	9	10	11	12	13	14	15
SiO_2 %	39.51	39.61	38.72	40.03	39.91	40.25	40.48	40.21	41.28	38.19	38.70	38.12	38.62	38.44	38.04
Cr_2O_3	0.00	0.00	0.01	0.01	0.02	0.03	0.04	0.04	0.07	0.02	0.11	0.08	0.06	0.07	0.04
FeO*	8.08	8.16	11.42	11.25	9.97	9.62	8.38	8.06	6.81	14.85	8.42	9.13	10.33	8.14	14.50
MgO	50.67	50.77	46.32	47.43	48.61	48.89	50.78	51.69	50.51	43.88	48.71	48.30	48.10	52.66	45.26
MnO	0.11	0.09	0.12	0.16	0.15	0.13	0.12	0.10	0.08	0.14	0.15	0.15	0.15	0.13	0.14
NiO	0.20	0.19	0.09	0.17	0.18	0.10	0.18	0.16	0.36	0.15	0.25	0.15	0.15	0.15	0.10
Na_2O	0.02	0.00	0.03	0.02	0.01	0.03	0.02	0.02	0.01	0.02	0.00	0.01	0.01	0.03	0.00
CaO	0.04	0.05	0.19	0.22	0.26	0.13	0.17	0.05	0.14	0.29	0.13	0.15	0.20	0.08	0.24
Fo	91.8	91.8	87.8	88.3	89.7	90.1	91.5	92.0	93.0	84.0	91.2	90.4	89.20	92.00	85.20

1, 2 olivine in crystal clots in picrite (D14-4), *3–9* D14-4 picrite phenocrysts, *10* D14-4 picrite groundmass, *11–14* D14-1 ankaramite phenocrysts, *15* D14-1 ankaramite groundmass

Table 2 Representative CPX analyses (cores)

	1	2	3	4	5	6	7	8	9	10	11	12	13	14	15
SiO_2 %	54.03	53.80	52.82	51.83	50.89	52.48	52.63	51.76	52.00	50.80	51.74	51.06	55.44	52.87	49.33
TiO_2	0.16	0.16	0.13	0.18	0.24	0.14	0.12	0.18	0.18	0.18	0.13	0.19	0.12	0.18	0.44
Al_2O_3	1.19	1.30	1.19	2.31	2.84	1.33	1.66	1.91	2.21	2.22	1.45	2.22	1.56	1.53	3.96
Cr_2O_3	0.31	0.37	0.85	0.57	0.39	0.98	0.82	0.62	1.40	1.09	0.56	0.88	0.81	0.18	0.17
FeO*	2.01	1.91	2.80	3.48	3.94	2.73	3.11	3.46	3.56	3.52	3.40	3.49	2.86	4.42	5.41
MgO	18.14	18.02	18.35	17.16	16.69	17.91	17.69	17.54	17.58	17.18	18.49	17.09	16.19	18.18	16.39
MnO	0.08	0.07	0.05	0.07	0.14	0.09	0.11	0.07	0.08	0.07	0.08	0.07	0.07	0.08	0.12
Na_2O	0.10	0.12	0.11	0.12	0.08	0.11	0.10	0.11	0.10	0.11	0.13	0.10	0.12	0.13	0.13
CaO	24.18	24.45	22.25	22.62	23.13	22.71	22.51	22.43	21.77	21.82	21.42	21.73	22.16	21.09	21.20
Wo	47.42	47.92	44.54	45.96	46.79	45.65	45.43	45.30	44.43	45.00	43.00	45.10	47.20	42.30	44.00
En	49.50	49.15	51.09	48.52	5.51	6.22	4.28	49.30	4.90	49.30	51.70	49.30	48.00	50.80	47.30
Fs	3.08	2.93	4.37	5.51	6.22	4.28	4.90	5.50	5.67	5.70	5.30	5.60	4.80	6.90	8.80
Mg#	94.14	94.37	92.12	89.80	88.31	92.12	91.03	90.00	88.81	89.70	90.70	89.70	91.00	88.00	84.40

1,2 CPX in crystal clots in picrite, *3–8* picrite phenocrysts, *9* picrite groundmass, *10–14* ankaramite phenocrysts, *15* ankaramite groundmass

Table 3 Representative spinel analyses

	1	2	3	4	5	6	7	8	9	10
SiO_2 %	0.00	0.01	0.02	0.02	0.03	0.01	0.06	0.03	0.02	0.13
TiO_2	0.39	0.41	0.26	0.37	0.37	0.35	0.37	0.35	0.40	0.46
Al_2O_3	20.58	18.41	12.45	11.75	11.60	11.89	10.77	17.14	12.42	15.26
Cr_2O_3	39.31	40.93	47.74	41.20	40.99	40.79	53.85	43.56	47.65	46.96
Fe_2O_3	12.52	2.13	3.48	17.55	16.76	15.74	9.25	12.56	13.09	10.60
FeO	12.86	23.76	18.91	15.05	15.31	15.81	11.51	9.84	12.07	10.12
MgO	14.76	13.66	15.79	12.50	12.73	12.94	14.78	16.24	14.40	16.00
MnO	0.17	0.23	0.28	0.23	0.21	0.21	0.17	0.22	0.24	0.18
V_2O_3	0.12	0.09	0.05	0.12	0.12	0.11	0.06	0.12	0.13	0.12
ZnO	0.13	0.20	0.14	0.09	0.20	0.15	0.02	0.09	0.04	0.11
Cr#	0.56	0.60	0.72	0.70	0.70	0.70	0.77	0.63	0.72	0.67
Mg#	0.93	0.93	0.87	0.59	0.60	0.62	0.70	0.75	0.68	0.74

1 spinel in crystal clot, *2–6* spinel as phenocryst, *7–10* spinel included in olivine

equilibrium with an evolving lava that includes the bulk compositions (Fig. 2b). The olivine compositions off the trends are likely cumulates from fractionated or mixed liquids. As in Fig. 2a, the data indicate that the primary MI hosts are in equilibrium and thus should preserve a record of the parental magmas.

The spinels have TiO_2 contents of 0.24–0.28 wt% and $Fe^{2+/3+}$ values of 0.75–1.29 over 7.38–20.69 wt% Al_2O_3 (Fig. 3a, b), within the range of magmatic spinel characteristics of the island arc and MORB provenances as defined by Kamenetsky et al. (2001). Included spinels have Cr#s at the host Fo contents within the
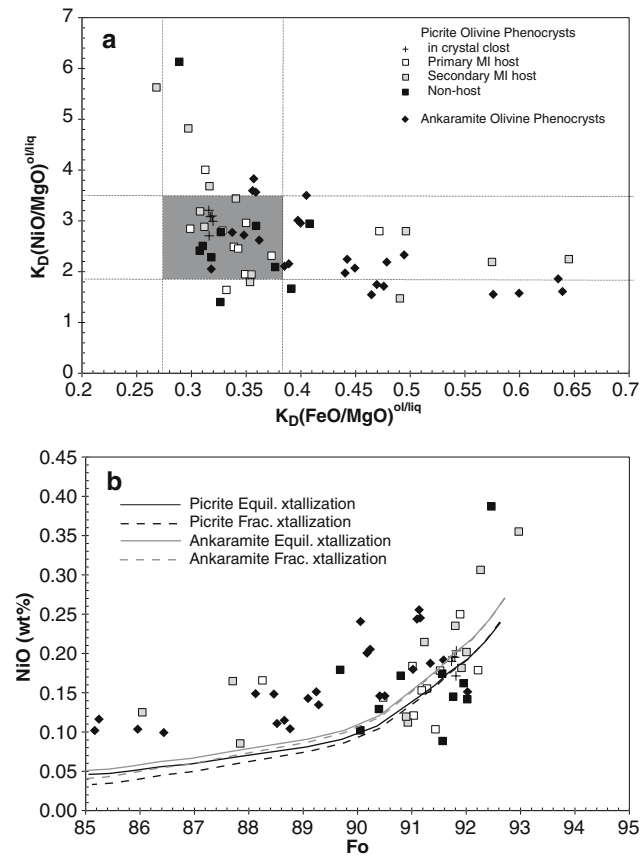
Fig. 2 **a** NiO/MgO and FeO/MgO partitioning between olivine and whole rock compositions for Chaife lavas. *Dashed lines* bracket equilibrium $K_D(FeO/MgO)^{ol/liq}$ and $K_D(NiO/MgO)^{ol/liq}$ defined by Takahashi (1978); *gray field* is where the olivines are in equilibrium with host lava. Picrite (D14-4) olivine phenocrysts are divided into those in crystal clots, phenocrysts and phenocrysts hosting either primary or secondary melt inclusions (*MI*). While a number of olivines are not in equilibrium with the bulk lava compositions and are likely accumulated, equilibrium olivines are present and include many of the hosts for primary melt inclusions. **b** NiO vs. Fo content for olivine (symbols as in **a**). *Solid lines* mark equilibrium crystallization paths and *dashed lines* mark fractional crystallizations paths for picrite and ankaramite olivines. Scattered compositions away from trends are the possible cumulate olivines

mantle array of Arai (1994), suggesting that the spinel and olivine crystallized from melts in equilibrium with the mantle peridotite (Fig. 3c). The spinel included in olivine has a limited compositional range, and the trend of spinel Mg# decrease with host olivine Fo (Fig. 3d) is within the range of the mantle peridotite as reported by Kamenetsky et al. (2001). This indicates that the spinel and olivine co-precipitated as the melt underwent a limited amount of evolution and the olivine–spinel pairs did not result from the widely different mantle sources or magmas. It is possible that the spinel Mg#–olivine Fo trend reflects some diffusive re-equilibration between the olivine and spinel (Dick

and Bullen 1984; Ballhaus et al. 1991; Scowen et al. 1991). For this reason we consider the Kamenetsky et al. (2001) method utilizing spinel Al_2O_3 vs. TiO_2 (Fig. 3a) as a more reliable means to indicate the tectonic setting and to distinguish the magmatic from peridotite spinels.

The groundmass for picrite has a $^{40}Ar/^{39}Ar$ plateau age of 2.49 ± 0.18 Ma while the ankaramite groundmass was dated at 1.73 ± 0.06 Ma. In comparison, the present Mariana volcanic arc is considered to have initiated at 3–4 Ma. This constraint is provided by the rifting that produced the currently active Mariana Trough, which disrupted the active arc at that time and forced a new arc to form at its present site (Stern et al. 2003).

Major element compositions

The lavas we recovered have Mg#s (assuming all Fe as FeO) of ~76 (Table 4) and both lavas can be classified compositionally as picrite (LeBas 2000); however, we will continue to use the textural classifications throughout this paper to distinguish the two mineralogically different lavas. Picrite (D14-1) contains 14.9% MgO, < 2 wt% total alkalis, 10.3% Al_2O_3 and 0.5% TiO_2 with CaO/Al_2O_3 of 1.35 (Table 4). Ankaramite (D14-4) is virtually identical in composition with picrite, with slightly higher Mg#s and a CaO/Al_2O_3 of 1.55–1.41 (Table 4). The average composition of the picrite groundmass glass is 7.97 wt% MgO (Mg# of 60.1), 15.26 wt% Al_2O_3, 0.71 wt% TiO_2 and 2.20 wt% total alkalis. There is no glass in the ankaramite groundmass to analyze. Both lavas have Cr contents > 400 ppm and Ni contents of 187 and 214 ppm (Table 4) that are consistent with those considered typical for the presumed primary magmas.

Few olivines host MIs (~10%) and we concentrated our MI analyses on the picrite (D14-4), which provided more inclusions simply due to its greater abundance of olivine. We targeted primary inclusions that formed while the crystal was growing (Roedder 1984) and presumably trapped equilibrium melts. MIs were considered primary if they occurred near the phenocryst core and were rounded with no evidence of resorption. Inclusions meeting these criteria were found to require < 15% olivine correction. Irregular shaped inclusions and those near the host rim were considered to be possible secondary inclusions formed by dissolution after crystallization and thus would not contain equilibrium melts. More detail on the morphology of secondary and primary inclusions in olivine may be found in Faure and Schiano (2005) and Kohut and Nielsen (2004).
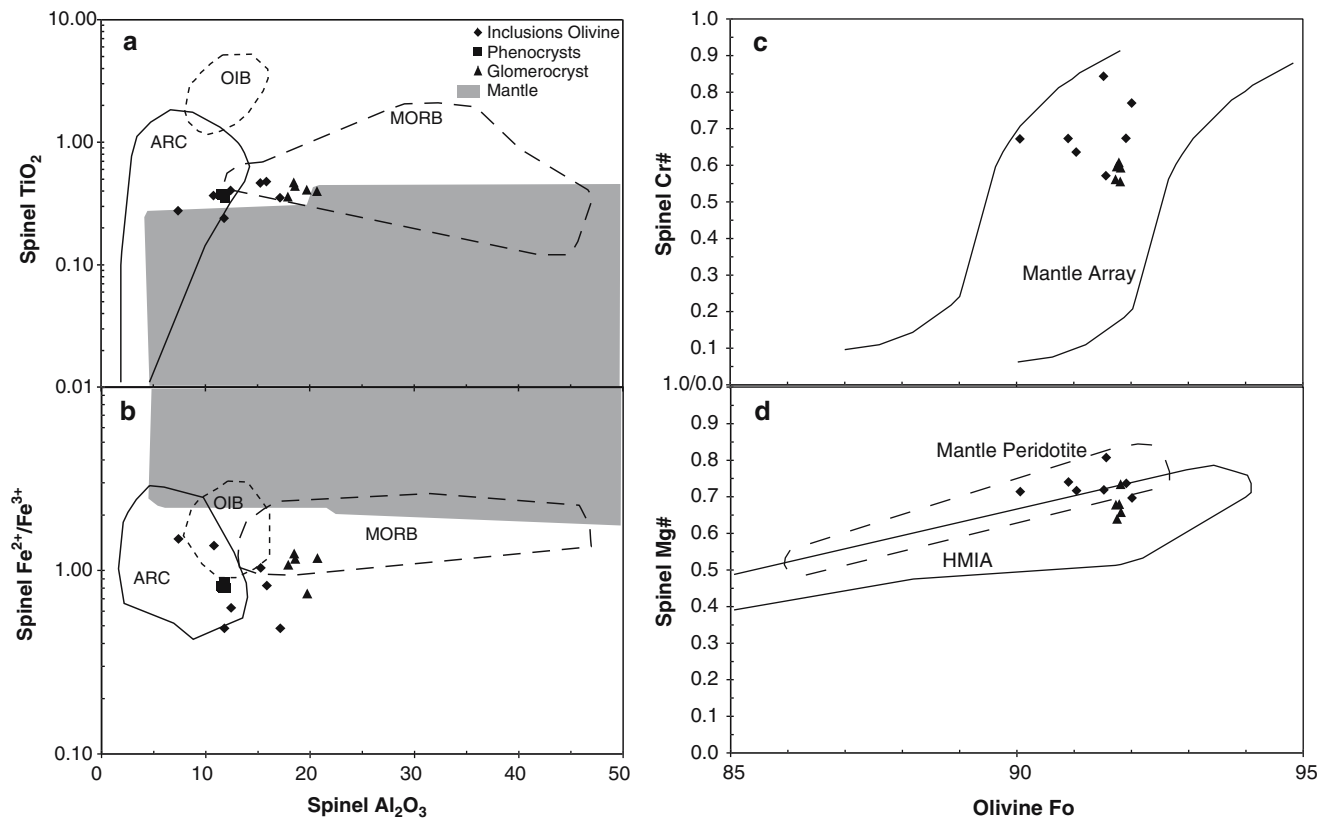
Fig. 3 a Picrite (D14-4) spinel TiO_2 vs. Al_2O_3. **b** $Fe^{2+/3+}$ vs. Al_2O_3. Spinels are phenocrysts, included in olivines or in the 0.8 cm olivine–CPX–spinel clot (see text). The only spinels in the ankaramite are the groundmass spinel and are too small to effectively analyze. *Black lines* denote magmatic spinel (arc, OIB and MORB) and the *gray field* is the mantle peridotite spinel as described in Kamenetsky et al. (2001). Note that the data point to the spinel is magmatic in origin (similar to both typical MORB and arc spinels) and not mantle xenocrysts. **c.** Spinel Cr# vs. host olivine Fo (for the included spinel) or adjacent olivine for the spinel from crystal clot. Mantle array after Arai (1994). **d** Spinel Mg# [$Mg/(Fe^{2+}+ Mg)$] vs. host olivine Fo. Fields for mantle peridotite and high-mg island arc (HMIA) lava based on data in Kamenetsky et al. (2001). Chaife Olivine-spinel pairs have a narrow compositional range and indicate equilibrium with mantle melts

In general, MI compositions are more primitive than the host lava, with median Mg#s of 77.0 and a maximum of 79.5. The majority of corrected MI compositions have 17.17–17.86% MgO (Table 5). The MI compositions are similar in respects to both the Pacific Ocean Island and Mariana arc basalts in the Georoc database (http://www.georoc.mpch-mainz.gwdg.de/georoc) (Fig. 4). It is noteworthy that the Chaife MIs are distinctly more magnesian than most primitive arc lavas (see Table 1 of Gaetani and Grove 2003). It is also worth noting here that the lavas and MI do not share major element characteristics with boninites, another unusual magnesian, although more silicic, lava found in the IBM arc system. Although generally not as magnesian as komatiites (Le Bas 2000) the Chaife melts do have similarly low Al_2O_3 concentrations (Fig. 4).

A number of corrected MI compositions had > 20% MgO. Many of these have been discounted due to either the large amount of added olivine needed to achieve host/inclusion equilibrium (> 30%), FeO contents >> whole rock, or morphologies that suggested that they were secondary inclusions. However, we still include in our data set a few high-MgO MIs (6,7 and 9—Table 5). These MIs met the criteria described above and those in Roedder (1984) for the primary inclusions.

Picrite and MI normative assemblages are hypersthene-normative olivine tholeiites. These plot close to the critical plane of silica undersaturation on the basalt tetrahedron (Yoder and Tilley 1962). Normative compositions of whole rock picrite correlate with the MI norms, whereas the ankaramites are slightly more diopside normative.

Isotopic and trace element compositions

Overall, the Chaife lavas are isotopically similar to the typical Mariana arc lavas (Stern et al. 2003), which indicates that they are derived from a similar mantle

Table 4 Chemical composition of Chaife seamount lavas

	D14-1-4 Ankaramite	D14-1-5 Ankaramite	D14-4-1 Picrite	D14-4-2 Picrite	D14-4 GM	2σ
SiO_2 %	48.24	47.94	48.52	48.70	50.08	0.85
TiO_2	0.47	0.47	0.48	0.49	0.71	0.03
Al_2O_3	9.09	9.94	10.29	10.30	13.72	0.92
FeO*	8.21	8.22	8.35	8.33	9.40	0.84
MgO	15.36	15.23	14.95	14.80	7.97	0.75
MnO	0.15	–	0.15	0.15	0.14	0.04
K_2O	0.52	0.53	0.42	0.42	0.60	0.10
Na_2O	1.43	1.41	1.38	1.28	1.58	0.27
CaO	14.09	14.04	13.90	13.98	16.45	0.51
P_2O_5	0.09	0.09	0.10	0.09	0.15	0.03
Total	97.65	97.87	98.54	98.54	100.87	
Mg#	76.93	76.76	76.15	76.01	60.10	
CaO/Al_2O_3	1.55	1.41	1.35	1.36	1.20	
Sc (ppm)	55	54	54	54	–	
V	230	229	231	235	–	
Cr	–	808	875	–		
Co	–	53	49	–	–	
Ni	–	214	187	–	–	
Cu	–	52	80	–	–	
Zn	–	77	93	–	–	
Rb	–	5	8	–	–	
Sr	328	327	339	340	–	
Y	9	9	10	10	–	
Zr	24	22	25	21	–	
Nb	–	1	1	–	–	
Cs	–	0	0	–	–	
Ba	86	87	89	87	–	
La	–	3.8	4.0	–	–	
Ce	–	8.6	12.6	–	–	
Pr	–	1.2	1.2	–	–	
Nd	–	5.7	5.9	–	–	
Sm	–	1.6	1.7	–	–	
Eu	–	0.6	0.6	–	–	
Gd	–	1.9	1.9	–	–	
Tb	–	0.3	0.3	–	–	
Dy	–	1.8	1.8	–	–	
Ho	–	0.4	0.4	–	–	
Er	–	1.1	1.1	–	–	
Tm	–	0.2	0.2	–	–	
Yb	–	1.0	1.0	–	–	
Lu	–	0.2	0.2	–	–	
$^{87}Sr/^{86}Sr$	0.703362	0.703359	0.703306	0.703303		
$^{143}Nd/^{144}Nd$	0.512938	0.512977	0.512952	0.512971		
ϵNd	6.06	6.82	6.35	6.71		
$^{176}Hf/^{177}Hf$	–	0.283185	0.283190	–		
ϵHf	–	14.59	14.77	–		
$^{206}Pb/^{204}Pb$	19.02	19.05	19.02	–		
$^{207}Pb/^{204}Pb$	15.56	15.59	15.60	–		
$^{208}Pb/^{204}Pb$	38.54	38.60	38.66	–		
$\Delta7/4$	0.90	2.93	4.28	–		
$\Delta8/4$	–8.86	–5.18	3.99	–		
Age	1.76 ± 0.06 Ma	2.49 ± 0.18 Ma				

GM is average groundmass glass composition. 2σ is standard deviation for GM composition

source. The $^{87}Sr/^{86}Sr$ values (Table 4) average from 0.70330 (ankaramite) to 0.70336 (picrite). This falls within the range of 0.7030–0.7040 for the IBM system, and are greater than that of N-MORB (~0.7028—Ito, 1982) or Mariana Trough back-arc basin basalts (BABB) (~0.70304—Stern et al. 2003). The ϵNd values are + 6.1–6.8, which are lower than MORB or BABB, but are again typical for Mariana magmatic front lavas (mean of + 6.7). The $^{206}Pb/^{204}Pb$ values of 19.015–19.047 are slightly more radiogenic than the IBM

Table 5 Melt inclusion compositions

	1	2	3	4	5	6	7	8	9	10	11	12	13
SiO_2 %	50.59	48.07	48.23	47.72	47.28	46.38	45.36	47.37	42.31	47.27	47.14	47.27	47.37
TiO_2	0.50	0.36	0.45	0.47	0.48	0.35	0.37	0.49	0.40	0.45	0.47	0.47	0.46
Al_2O_3	7.18	13.25	9.52	9.02	9.06	8.67	7.56	10.01	10.23	9.1	9.14	8.93	8.97
Cr_2O_3	0.04	0.00	0.04	0.06	0.08	0.04	0.17	0.04	0.00	0.07	0.05	0.06	0.04
FeO	8.75	8.85	8.66	8.85	9.15	10.69	11.38	9.05	10.72	9.12	9.06	9.16	9.05
Fe_2O_3	1.98	1.41	0.40	1.36	1.41	1.41	1.70	1.41	1.60	1.42	1.39	1.36	1.36
MgO	11.95	15.31	17.86	17.18	17.40	22.53	22.91	17.17	23.65	17.33	17.22	17.44	17.18
MnO	0.20	0.10	0.15	0.20	0.19	0.17	0.24	0.12	0.18	0.11	0.13	0.18	0.17
K_2O	0.26	2.25	0.44	0.45	0.46	0.50	0.21	0.49	0.48	0.47	0.48	0.45	0.47
Na_2O	1.58	2.01	1.43	1.45	1.43	2.05	1.10	1.41	1.47	1.50	1.44	1.44	1.43
CaO	16.72	8.19	13.05	13.1	13.17	7.12	8.87	13.28	8.82	13.08	13.4	13.13	13.61
P_2O_5	0.26	0.21	0.13	0.14	0.13	0.09	0.12	0.09	0.13	0.12	0.11	0.14	0.13
S (ppm)	51	2,102	1,362	1,615	1,413	53	2,022	2,420	0	1,077	1,656	1,419	1,381
Cl (ppm)	5	248	210	209	334	13	1346	313	0	249	324	226	182
Total	100.0	100.0	100.4	100.0	100.2	100.0	100.0	100.9	100.0	100.0	100.0	100.0	100.2
Mg#	70.6	75.3	78.4	77.4	77.0	78.8	78.0	77.0	79.5	77.0	77.0	77.0	77.0
CaO/Al_2O_3	2.33	0.62	1.37	1.45	1.45	0.82	1.17	1.33	0.86	1.44	1.47	1.47	1.52
Host Fo	88.6	91.1	92.9	92.2	92.1	92.8	92.7	90.4	92.7	92.1	92.0	92.1	92.1
% Ol added	0.87	14.18	15.63	3.44	3.47	6.38	-8.25	2.08	10.83	1.87	3.36	7.41	6.24
T^{RH}	1,200	1,200	1,200	1,250	1,250	1,250	1,250	1,250	1,200	1,250	1,250	1,200	1,200
Rb (ppm)	9	7	6	8	10	11	5	4	7				
Sr	264	250	338	403	354	359	263	210	310				
Y	27	17	17	12	9	8	10	6	11				
Zr	92	53	51	26	20	21	29	17	28				
Nb	3	1.31	1.25	0.90	0.70	0.68	0.76	0.56	0.95				
Ba	173	62	84	87	84	83	68	63	93				
La	9	4	5	4	3	4	4	3	5				
Ce	20	11	11	9	9	9	9	7	10				
Pr	3	2	2	1	1	1	1	1	1				
Nd	14	7	9	7	6	6	6	4	7				
Sm	4	3	3	2	1	1	1	1	2				
Eu	1	1	1	1	0	1	0	0	1				
Gd	3.9	2.4	3.0	2.1	1.6	1.3	*BDL	*BDL	1.8				
Dy	4.0	3.2	3.1	1.8	1.4	1.4	1.6	1.2	1.5				
Er	2.6	1.5	1.9	1.2	0.9	0.8	1.2	0.6	0.8				
Yb	2.9	2.07	1.54	1.24	0.82	0.78	1.23	0.67	1.06				
Hf	2.0	1.1	1.5	0.9	0.4	0.6	0.7	*BDL	0.7				
Ta	*BDL	0.0	0.1	0.1	*BDL	*BDL	*BDL	*BDL	*BDL				
Pb	3.6	0.4	0.7	1.5	1.2	1.4	0.3	*BDL	*BDL				
Th	1.2	0.4	0.5	0.3	0.4	0.4	*BDL	0.3	0.5				
U	0.4	0.2	0.8	0.1	0.2	0.2	*BDL	*BDL	0.3				

T^{RH} is the rehomogenization temperature

% Ol added is the amount of olivine added to the melt inclusion composition to achieve equilibrium with the host

system mean of 18.85. The Δ7/4 and Δ8/4 values (Table 4) indicate deviations from the Northern Hemisphere Reference Line (NHRL) of Hart (1984) that describes the Pb isotopic characteristics of non-subduction related oceanic volcanoes. The picrite has a Δ7/4 of 4.28, which is not substantially different than the mean Δ7/4 for the IBM system (4.4), while the ankaramite Δ7/4 values are significantly lower at 0.9–2.9 (Table 4). The Δ8/4 values are also different between the two lavas, with +4.0 for the picrite and –8.9 to –5.2 for the ankaramite. The Δ8/4 values are less diagnostic for contributions from the subducted sediments, and might reflect differences in mantle domains. However, based on the parameters defined in Pearce et al. (1999), the $^{176}Hf/^{177}Hf$ and ϵHf data are consistent with the Indian Ocean type mantle that IBM magmas have tapped for the past 50 Ma. The Indian-Pacific mantle boundary lies at ϵHf = 1.6 × ϵNd (Pearce et al. 1999), and the Chaife lava ϵHf are equivalent to 2.14–2.33 × ϵNd, well within the Indian domain. Thus the differences in Δ7/4 and Δ8/4 between the two lavas likely reflect a smaller subduction signal in the ankaramite rather than differences in the mantle source domains.

Trace element concentrations for Chaife whole rocks normalized to primitive mantle have patterns similar to typical basaltic arc lavas (Fig. 5a). The LILE
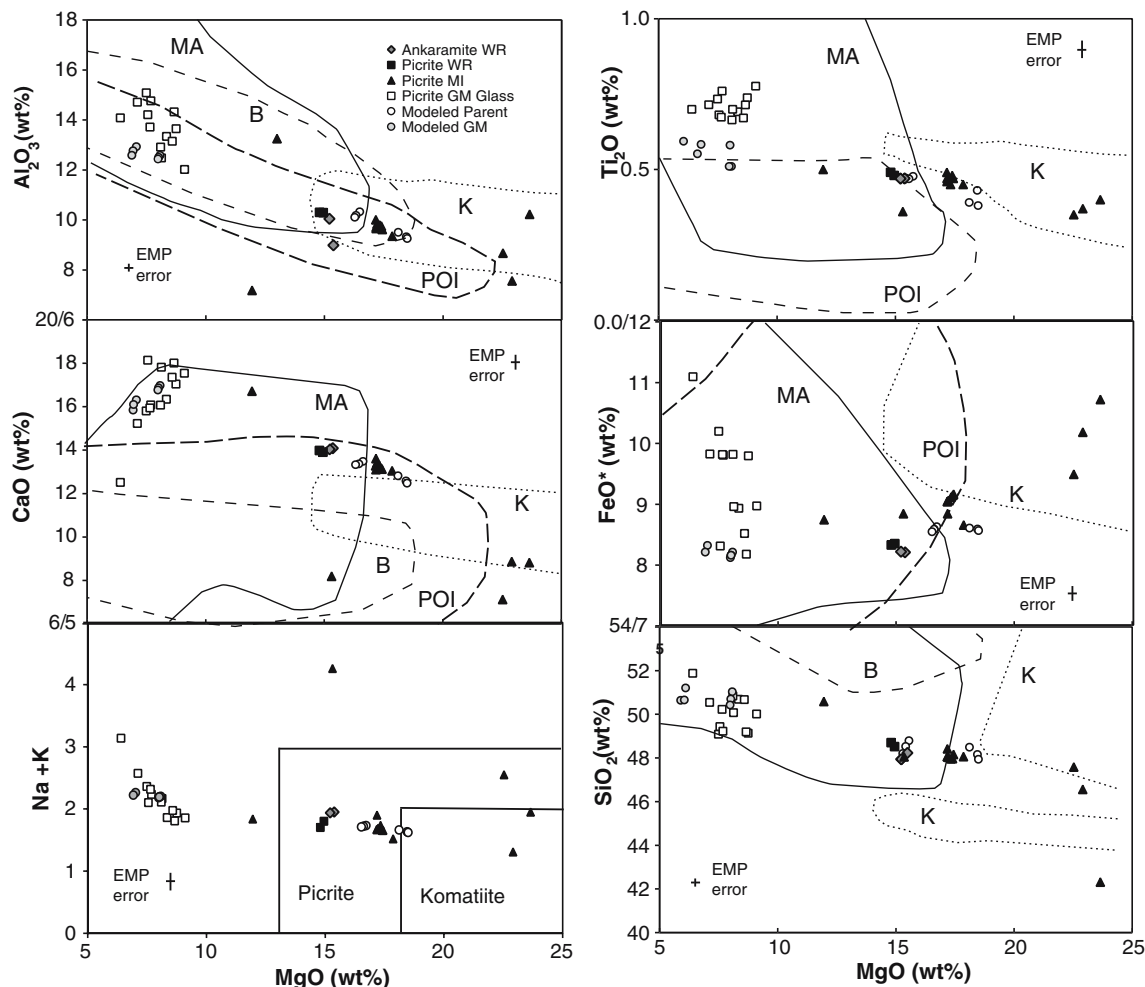
Fig. 4 Variation of major element compositions with MgO. *MI* melt inclusions. *MA* Mariana arc lavas (*solid line*), *POI* Pacific Ocean islands (*long dashed line*), *B* boninites (*short dashed line*) and *K* komatiites (*dotted line*). On the Na + K vs. MgO plot, picrite and komatiite fields are from the IUGS classification scheme (Le Bas 2000). Petrolog GM is the calculated groundmass composition for the picrite, and Petrolog parent is the calculated parent magma. *Error bars* refer to the analytical relative error

(measured-true/measured) for EMP analyses of melt inclusions. Most MI compositions fall along trends through the lava to groundmass glass compositions. This indicates a genetic relationship and melt included in olivine phenocrysts are parent magmas for the picrite. Chaife lavas and MIs have lower total alkalis than the other comparable arc picrites and can be classified chemically as picrite and komatiite

are especially enriched relative to MORB and the HFSE, while Nb and Ta are depleted. These whole rock samples have a restricted range in primitive mantle-normalized abundances and overlap the more depleted MIs (Fig. 5b). No MI examined has a distinctively MORB or OIB-like pattern. In a few of the most depleted MI, the trace element patterns lack the characteristic Pb spike of island arc basalts. The MI with the highest normalized trace element concentrations of Ba, Rb, U and Pb are also those with the highest alkalis (1,2,6—Table 5).

The Chaife whole rock samples are similar to the typical Mariana arc magmas in terms of key trace element ratios (Th/Yb, Zr/Yb, Nb/Yb, Th/Nb, Ba/Th, U/Th and Pb/Ce; Fig. 6). The co-variation of trace

element ratios was examined to determine the relative contribution of subduction-derived components to the melts. Ratios of trace elements conserved in the downgoing slab to those that are released during subduction (non-conservative) provide measures of the subduction component in a melt (Pearce and Peate 1995). We compared Th (non-conservative) to Nb (conservative) which indicates the relative depletion of the mantle source (Fig. 6a). These concentrations are Yb normalized after the practice of Pearce and Peate (1995) to minimize partial melting and fractionation effects. The range of Nb/Yb in the MIs is ~0.6–1, similar to N-MORB (Pearce and Peate 1995). The Th/Yb values in most MIs are elevated relative to the mantle and are interpreted as an added subduction

Fig. 5 Spider diagram of primitive normalized whole rock (**a**) and MI (**b**) trace element concentrations. All have an arc-like signature, but at lower concentrations than most arc lavas. The most depleted MIs have a negative Pb anomaly and Nb contents below the primitive mantle, similar to N-MORB. N-MORB from McDonough and Sun (1995), global subducting sediment (*GLOSS*) from Plank and Langmuir (1998), island arc basalt from Peate et al. (1997) and Taylor and Maclennan (1995)
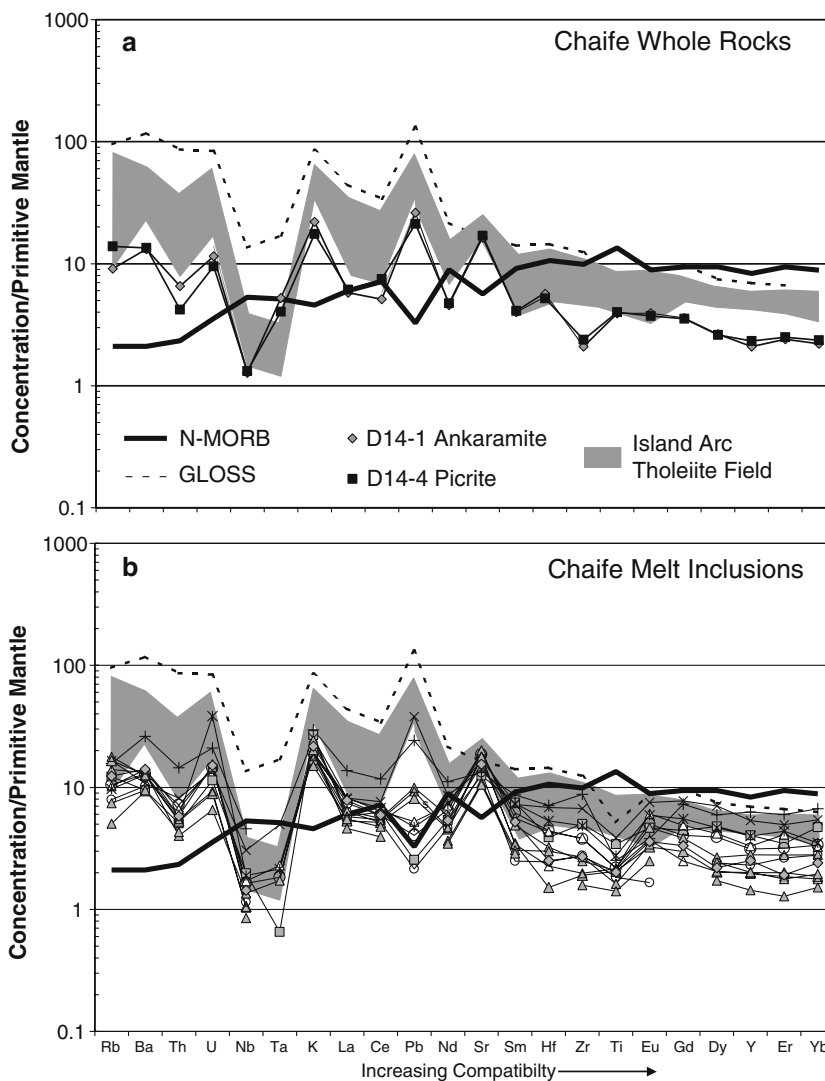
component. The lack of Zr/Yb enrichment above the mantle array (Fig. 6b) indicates that slab melting did not take place (Pearce and Peate 1995), and the subduction component was instead derived from sediment melt and/or aqueous fluid.

The relative contributions of aqueous fluid and sediment were examined by comparing Th/Nb to Ba/Th, U/Th and Pb/Ce (Fig. 6c–e). Barium and Pb are present in the sediment, but can also be mobilized by fluid. Uranium is enriched in aqueous fluids (Hawkesworth et al. 1997), while in contrast Th is present in the subducted sediment but is generally not thought to be mobilized by aqueous fluids. Elevated Th/Nb is thought to result from sediment melting (Johnson and Plank 1999), while elevated Pb/Ce and Ba/Th could arise from either aqueous fluids or sediment melts (Elliot et al. 1997; Class et al. 2000). MI compositions show a large and continuous Th/Nb trend within the range typical of island arc tholeiites (Taylor

and Mclennan 1995), including Mariana arc lavas (Bryant et al. 2002). Ba/Th and Pb/Ce vary directly with Th/Nb, while U/Th does not vary much over the large range seen for Th/Nb. U/Th, Pb/Ce and Ba/Th each have strong enrichments in different inclusions analyzed by LA–ICP-MS, possibly due to differing effects of fluid contribution (Fig. 6c–e). The Th and U data thus indicate contributions from both the sediment and fluid, with the sediment signal persisting in a wider range of MI compositions. In general, Chaife lavas have a smaller range in these key trace element ratios, but overlap the MI data (Fig. 6).

Also, note that the MI and Chaife lavas form a positive trend on the Ba/Th vs. Th/Nb plot (Fig. 6c), whereas the Mariana frontal arc magmas show a trend of decreasing Ba/Th with increasing Th/Nb. The latter suggests mixing between fluid dominated and sediment-melt dominated contributions to the mantle wedge. The Chaife MIs appear to represent a trend to a
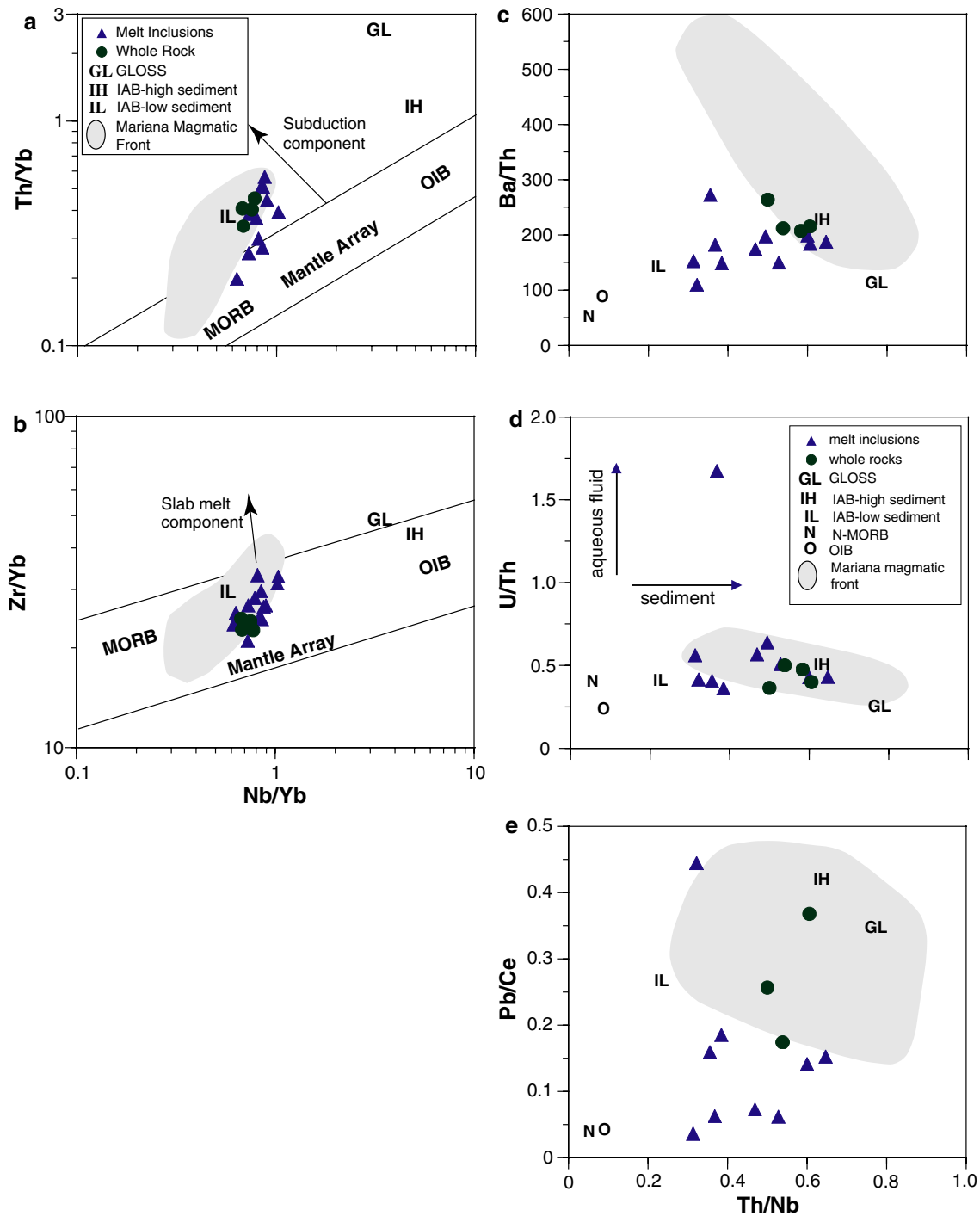
Fig. 6 **a** Th/Yb variation with Nb/Yb; elevated Th/Yb above the mantle array indicates the addition of a subduction component, **b** Zr/Yb variation with Nb/Yb; elevated Zr/Yb above the mantle is evidence for slab melt. Nb/Yb shows relative mantle enrichment. Most MIs have a Th signature that suggests sediment participation, but no evidence of slab melt. **c–e** Aqueous fluid and sediment-derived (potentially sediment melt) components

in MI compositions. Only a few MIs have a mild fluid enrichment signal, most have some sediment signal. Sediment and fluid enrichment do not correspond. Mariana arc field (enclosed by *dashed line*) from the data in Bryant et al. (2002). IAB-island arc basalts with high and low subduction components, *GLOSS* global subducting sediment, references are the same as in Fig. 5

Table 6 FTIR and EMP data for the unheated inclusions

	1	2	3	4	5	6
SiO_2 %	51.93	51.17	53.24	44.06	47.15	50.09
TiO_2	0.67	0.61	0.71	0.48	0.59	0.64
Al_2O_3	17.11	10.37	15.16	12.80	11.96	13.36
Cr_2O_3	0.01	0.62	0.05	0.03	0.01	0.02
FeO*	8.11	9.38	6.77	13.43	11.23	9.44
MgO	7.43	11.60	5.07	14.12	8.43	12.10
MnO	0.20	0.13	0.16	0.16	0.16	0.14
K_2O	1.06	0.56	1.03	0.53	0.74	0.32
Na_2O	2.93	1.43	2.50	1.47	1.48	1.80
CaO	11.48	16.19	15.60	12.96	16.50	12.72
P_2O_5	0.30	0.10	0.19	0.12	0.17	0.09
S (ppm)	96	2,426	880	1,565	2,268	1,360
Cl (ppm)	57	318	422	242	443	410
H_2O %	0.11	0.64	0.54	0.49	0.34	0.43
Total	101.34	103.08	101.15	100.83	99.03	101.33
Mg#	53.57	56.09	36.67	66.01	47.66	62.90
Host Fo	89.92	91.52	91.91	91.01	92.97	89.50

less modified MORB type mantle, similar to what the Th/Yb variations suggest.

Volatile contents

Chlorine contents are generally in the range of 182–334 ppm, although some are as high as 1,346 ppm (Tables 5, 6). Inclusions with very low Cl (< 100 ppm) also have low S (Tables 5, 6). These MIs have likely lost Cl and S as the result of breaching during re-heating (Nielsen et al. 1998). Sulfur contents of the unbreached inclusions range from 1,077 to 2,426 ppm (Tables 5, 6).

Water contents were measured via FTIR only in unheated inclusions (Table 6). We utilized the un-heated inclusions because initial FTIR analyses of the rehomogenized inclusions indicated that most lost volatiles during re-heating, as they contained < 0.1 wt% H_2O. The unheated MIs examined were glassy and appeared to have little post-entrapment crystallization. No halos of melt/vapor bubbles were observed around the inclusions. These unheated inclusions contained low, but detectable amounts of water from 0.16 to 0.64 wt%, with most in the range of 0.3–0.5 wt% (Table 6, Fig. 7). These concentrations are lower than the 0.6–4.0 wt% primary water contents estimated for most arc magmas (Sakuyama 1979; Danyushevsky et al. 1993; Gaetani et al. 1993; Sisson and Layne 1993; Newman et al. 2000). Cl contents do not vary to any appreciable degree in the MI analyzed by FTIR, although the data set is too small to assess possible correlations between water, Cl and S concentrations (Table 6). The Chaife MI water contents more closely resemble those of the MI from MORB or OIB than the Mariana arc, although they overlap

the low end of the range of the arc MI water data (Fig. 7).

Temperature, pressure and fugacity estimates

We estimated magmatic temperatures (Table 7a) for the lavas using olivine–spinel geothermometers (Fabriés 1979; Roeder et al. 1979; Ballhaus et al. 1991) and the olivine–liquid thermometer of Ford et al. (1983). The olivine–spinel geothermometry calculations are limited to the picrite, in which several of the olivines included spinel. (Olivine and spinel compositions used in the calculations are in Electronic Supplementary Material Appendix III.) The ankaramite lacked any spinel except in the groundmass. Estimates were made for each mineral pair at pressures of 1, 2 and 3 GPa to account for pressure dependence in the thermometers, but this resulted in only 30–40° higher calculated temperatures at 3 GPa compared to 1 GPa. The medians for the olivine–spinel pairs ranged from 1,154 to 1,399° (Table 7a). This large range may be due to the diffusive re-equilibration that may occur between olivine and spinel inclusions. The Ford et al. olivine–liquid thermometer calculated temperatures for the picrite up to 1,435°C, and up to 1,380–1,400°C for the ankaramite (Table 7a). Pressures were estimated using the CPX-liquid barometer of Putirka et al. (1996, 2003). The results indicate pressures of 1.01–1.47 GPa (Table 7b) at the temperatures estimated by the mineral geothermometers.

Oxygen fugacities were derived using the Ballhaus et al. (1991) method and the olivine–spinel pairs used for the geothermometry calculations. Fugacities were calculated for each mineral pair at 1–1.5 GPa. Estimated fugacities ranged from log ΔFMQ of + 0.82 to + 2.06

Table 7 Estimated magmatic T, P and $f\mathrm{O}_2$

	Median	Range	Method, comments
(a) Estimated magmatic temperatures (°C)	1,320	1,245-1,324	Ol–Sp geothermometry, Ol Mg# = 91.53 , Sp Cr# = 0.84
	1,154	1,125–1,161	Ol–Sp geothermometry, Ol Mg# = 92.01, Sp Cr# = 0.77
	1,391	1,304–1,456	Ol–Sp geothermometry, Ol Mg# = 91.92, Sp Cr# = 0.67
	1,344	1,336–1,420	Ol–Sp geothermometry, Ol Mg# = 90.89, Sp Cr# = 0.67
	1,263	1,223–1,314	Ol–Sp geothermometry, Ol Mg# = 91.28, Sp Cr# = 0.64
	1,399	1,376–1,435	Ford et al. (1983) Ol–liquid thermometer for picrite
	1,390	1,380–1,400	Ford et al. (1983) Ol–liquid thermometer for anakaramite
	1,442	1,418–1,477	Petrolog parental magma model

	Median	Range	Comments
(b) Estimated magmatic pressures (GPa)	1.17	1.03–1.47	Putirka CPX–liquid barometers, ankaramite
	1.24	1.01–1.41	Putirka CPX–liquid barometers, picrite
	0.51	0.46–0.67	Putirka CPX–liquid barometers, picrite GM

	1 GPa	1.2 GPa	1.5 GPa	Comments
(c) Estimated magmatic $f\mathrm{O}_2$ (Δlog FMQ) at 1.0–1.5 GPa	0.95	0.92	0.82	Ol Mg# = 91.53 , Sp Cr# = 0.84
	1.60	1.54	1.46	Ol Mg# = 92.01, Sp Cr# = 0.77
	1.89	1.84	1.76	Ol Mg# = 91.92, Sp Cr# = 0.67
	1.66	1.61	1.53	Ol Mg# = 90.89, Sp Cr# = 0.67
	2.06	2.00	1.93	Ol Mg# = 91.04, Sp Cr# = 0.64
	1.66	1.61	1.53	Median for each pressure

(Table 7c). The median fugacity (log ΔFMQ) was + 1.66 and 1.53 at 1 and 1.5 GPa, respectively. These estimates lie at the low end of the range of the other estimates of fugacity (ΔFMQ = +1 to + 3) for arc lavas and some arc picrites (Ballhaus et al. 1991; Eggins 1993).

Degree of melting

The co-variation of elements with differing compatibilities can show both the degree of melting (F) and the amount of depletion of the melt source. We estimated F using the Nb–Yb variation diagram due to its ability to resolve between F and source depletion (Pearce and Parkinson 1993). We calculated several melting curves using primitive mantle compositions (McDonough and Sun 1995) and 1, 2 and 5% depleted primitive mantle compositions and compared these to the MI data. Simple non-modal batch melting models were found to have the best fit to the MI compositions, which plotted between the melting curves for primitive mantle (McDonough and Sun 1995) and the 2% depleted primitive mantle on the Nb–Yb diagram. The data do not fit well to fractional mixing curves, but the accumulations of incremental fractional melts are approximated by batch melting models. Based on these models, F ranged from 5 to 50% (Fig. 8a). The data do not show significant scatter and plot along what may be interpreted as a single melting curve or several closely spaced curves. We also modeled curves for a variety of mantle types (primitive mantle, 0.5,

0.75 and 1% depleted primitive mantle, N-MORB source mantle and various types of amphibole bearing mantle); for clarity we show those curves that the data best fit. Some MI data fit melting curves for the primitive mantle that has been slightly depleted (0.75%), while other data fit a melting curve for a 2% depleted hornblende lherzolite (Fig. 8b). Using mineral-melt partition coefficients in the literature (Shimizu 1982; Fujimaki and Tatsumoto 1984; Kennedy et al. 1993; Beattie 1994; Forsythe et al. 1992; Schwandt and McKay 1998), bulk distribution coefficients of D_{Nb} of 0.022 and D_{Yb} of 0.08 were used to produce the hornblende lherzolite melting curve with the best fit to the MI data. This corresponded to a modal assemblage of 61% Ol, 28% OPX, 7% CPX, 2% hornblende and 2% spinel. MIs with the highest LILE, U/Th and Na plot along the hornblende lherzolite curve (Fig. 8b). Degrees of partial melting for these MIs based on this curve were ~6–25%. The rest of the MI data fell along the depleted primitive mantle curve and have estimated F values of 35–50%. It is important to note that indications of very high degrees of melting are from the very high-MgO inclusions that may be anomalous. The lowest degree melts are similar to the N-MORB composition, although the MI data as a whole do not fit the N-MORB source melting curves. The MI data suggesting the lowest degree melts (~5–6%) may instead represent melting of a different source than the other MIs and thus in actuality result from higher amounts of melting.
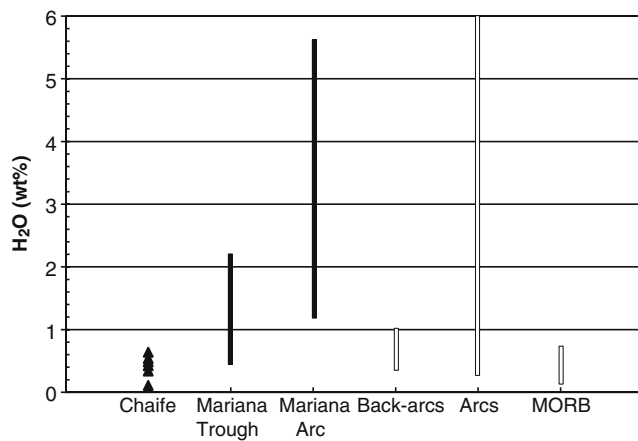
Fig. 7 Water content of the unheated inclusions analyzed by FTIR compared to the melt inclusion water data compiled by Newman et al. (2000). Chaife seamount melt inclusions contain significantly less water than typical for Mariana arc melt inclusions. The Chaife MI water contents are also significantly lower than the 1–3.2 wt% suggested for the boninite parental magmas (Crawford et al. 1989; Sobolev and Danyushevsky 1994;Dobson et al. 1995; Falloon and Danyushevsky 2000)

Discussion

Arc lavas are characteristically fractionated and the eruption of lavas with Mg#s > 70 is unusual. The generation of these high-MgO arc lavas has been attributed to a number of unique circumstances: early-arc magmatism and proximity to a triple junction (Hawkins 2003), arc–ridge collision (Baker and Condliffe 1996; Monzier et al. 1997), subduction of young crust (Schuth 2003), and melting during induced counterflow separate from a vertically rising diapir (Nye and Reid 1986). These particular circumstances and mechanisms largely do not apply to the genesis of the Chaife seamount lavas. The lithosphere in the Mariana subduction zone is among the oldest known (Hirschmann et al. 2000; Stern et al. 2003) and there is no collision between an arc and ridge in the trench to the east. With ages of 1.73 and 2.49 Ma, Chaife's lavas could be related to the creation of a new arc following back-arc rifting, and thus may be similar to the early-arc high-MgO tholeiites of Tonga (Hawkins 2003). However, this would require that arc reformation following back-arc rifting continued well after the inferred 3–4 Ma age of arc reformation (Stern et al. 2003).

What all the aforementioned models do have in common is an important role for adiabatic decompression melting. In common with the examples just described, Chaife lavas are very atypical for magmas originating along the volcanic front of an arc. Our estimated pressures of 1.0–1.5 GPa are fairly shallow
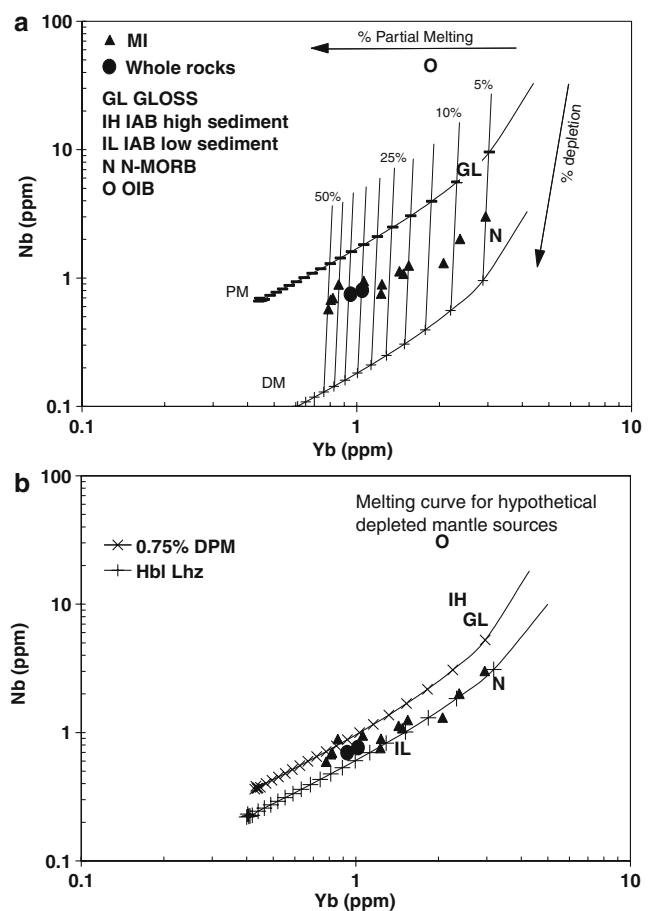

Fig. 8 Batch melting models compared to MI data on the Nb–Yb variation diagram. **a** MI data plot between the melting curve for primitive mantle (MacDonough and Sun 1995) and mantle depleted by 2% melting. **b** MI data compared to melting models for primitive mantle depleted by 0.75% melting (0.75% DPM) and similarly depleted hornblende lherzolite (Hbl Lhz). The majority of MIs plot along the hornblende lherzolite curve. Other MIs plot along the primitive mantle curve and have the highest F. The Nb and Yb concentrations for amphibole bearing mantle were taken from those given for hornblende lherzolite in Pearce and Parkinson (1993)

for such hot, magnesian melts, but these pressures reflect the last equilibration with the mantle, which may not be the melting conditions. A complicating factor is that the Putirka method for calculating magmatic pressures (Purtirka et al. 1996, 2003) requires a equilibrium CPX–liquid $K_D^{(Fe/Mg)}$ of 0.27 for the most accurate results and most CPX analyzed were not exactly in equilibrium with the bulk lava compositions. We suggest that the averaged estimated temperatures of 1,367°C at ~1.0–1.5 GPa suggests a geotherm perturbed by the upwelling hot asthenosphere beneath the magmatic arc at the Chaife seamount.

The H_2O contents of 0.11–0.64 wt% are consistent with the estimated oxygen fugacity (log ΔFMQ) of

+1.60, which lies at the low end of the range of other estimates of oxygen fugacity for arc lavas and some arc picrites (ΔFMQ = +1 to +3). This supports our contention that the magmas were water-poor initially and that the low water contents did not arise solely through dilution due to high degrees of melting. Furthermore, experimental studies (e.g. Gaetani and Grove 1998) indicate that the hydrous partial melting of peridotite produces liquids with elevated $SiO_2/(MgO + FeO)$ levels (>2.3). These values for the Chaife MI are 1.23–2.44 (median 1.79) and 2.04 for the whole rock, as expected for water-poor melts.

If these estimated P–T–fO_2 conditions and water contents are valid, then adiabatic decompression melting is the likeliest mechanism for generating the water-poor, high-MgO lavas. Nevertheless, Chaife lavas have trace element signatures that, although subdued, are diagnostic of subduction zone magmas. Thus, the Chaife magmas appear to have both subduction related and decompression melting signatures. This is supported by the spinel chemistries, which have Al_2O_3 and TiO_2 compositions similar to both typical island arc spinels and MORB spinels (Fig. 3a). Kamenetsky

et al. (2001) contend that these oxide concentrations are controlled by melt chemistry, which in turn is a function of the melting conditions and mechanisms. The degree of melting inversely correlates with the subduction component and this suggests control by dilution due to increased melting (Figs. 6, 8, Table 5). The observation that the bulk trace element concentrations are similar to the most depleted MI (Fig. 5) also supports the contention that the more LILE enriched MIs are samples of the earliest, lowest degree melts of a metasomatized mantle.

It is likely that bulk lava compositions reflect the effects of crystal accumulation to some extent, which can be observed in the disequilibrium nature of some of the olivine phenocrysts. The MI compositions are used as a means to circumvent this problem. To generate parental magma models for the picrite lava as comparisons to the MI, we utilized the parental melts for the picrites routine in Petrolog (Danyushevsky 2001). Intensive variables used in the model (P = 12 kbar, fO_2 of FMQ to log ΔFMQ = 1.6) were based on the data determined for the lavas using the mineral pairs and mineral-melt calculations. Full details of the model parameters and results are in Electronic Supplementary Material Appendix IV. The modeled parental magmas have ~16–18 wt% MgO and are similar in composition to most Chaife MIs (Fig. 3). Petrolog also produced groundmass compositions very similar to that of the picrite groundmass glass (Fig. 3). A trend from the theoretical parent to the modeled groundmass passes near or through the MI and bulk lava for most major elements and validates the inference that the MIs sample near primary magma compositions and the bulk compositions and groundmass lie on a liquid line of descent. The models provide higher temperature estimates (1,418–1,477°C) overall than the olivine–spinel and olivine–liquid geothermometers (Table 7). The Petrolog models should not be considered definitive, but instead provide a degree of constraint on the possible parental magmas for the Chaife lavas.

We envision a process that accounts for these compositions that while simple, also requires unusual conditions for a subduction zone (Fig. 9). In our model, the asthenopheric wedge is not only hydrated by fluids from the downgoing slab, but also experiences significant upwelling more typical of rift zones and hotspots. This upwelling, via decompression melting, is the source for Chaife melts. The observed subduction zone trace element signature (Figs. 5, 6) is imparted by the hydration of the mantle wedge prior to upwelling. Because magma generation does not arise directly as a result of fluxing from the subduction related fluids (e.g.
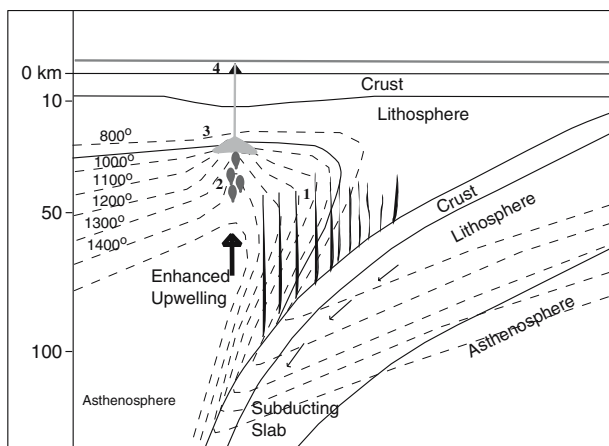

Fig. 9 Model for the magmagenesis of the Chaife lavas. The steep dip of the slab in the model and the crustal thickness are based on Figs. 11 and 13 in Stern et al. (2003). Geotherms are speculative, but are based on temperature data from geothermometry and geobarometry (see text) and models that allow for greater sub-arc temperatures (e.g. Tatsumi and Eggins 1995; van Keken et al. 2002). *1* Dehydration of the subducting slab hydrates forearc and descending limb of mantle wedge. *2* A typical upwelling (potentially related to slab tear) induces decompression melting in the partially metasomatized mantle wedge, producing the water-poor, high-MgO magmas with a subduction related trace element signature. The locally hot shallow geotherms reflect perturbations due to the rising hot melt. *3* Melt accumulates at the base of the lithosphere. *4* Magma from location 3 ascends to the surface without undergoing substantial low-pressure segregation or assimilation and erupts as high-Mg lava

due to the breakdown of phlogopite at depth), K_2O and other LILE contents in the magmas remain low. One major issue with this scenario is that it may require a higher than expected subduction zone geotherm if the highest estimates for the temperatures of the Chaife lavas (1,380–1,477°C—Table 7) are considered, although most of our estimated temperatures are similar to the temperature expected in the core of the mantle wedge. This also would suggest that, rather than providing an insight into the subduction magmagenesis in general, the Chaife lavas provide evidence of unusual tectonics in this part of the Mariana Arc. Recently, evidence of such conditions has been provided by other disciplines. Geophysical data suggest a tear or some other discontinuity in the subducted lithosphere directly beneath the Chaife seamount (Miller et al. 2004). This discontinuity causes the upper plate to rift above it, stimulating upwelling of the mantle wedge material. Melting need not occur at depths corresponding to the slab tear or discontinuity; rather it could occur between 30 and 60 km depth, well within the mantle wedge. Although we are not certain yet of the exact mechanism by which this slab tear could produce mantle upwelling, similar slab tears have been linked to atypical mafic magmatism within subduction zones, e.g. Mt. Etna (Gvirtzman and Nur 1999). For most arc volcanoes, parental melts are thought to segregate after the diapiric ascent stops at the base of the lithosphere and these melts then rise through the lithosphere. Melt separated from the crystal-rich magma would then be modified by assimilation, fractionation and mixing at shallow levels (< 1.0 GPa) to yield characteristic evolved arc magmas. However, it appears that below the Chaife seamount, magmatic fractionation was unusually limited. The reason why significant low-pressure segregation and modification did not occur is probably related to the anhydrous nature of Chaife melts. These melts were able to rise to shallow depths without the loss of water and attendant rapid crystallization. The anomalous tectonic setting may also have helped suppress fractionation; Nye and Reid (1986) postulate that Okmok high-MgO lavas reached the surface more readily due to the location of the volcano on a segment boundary. There is a WNW–ESE trending zone of crustal earthquakes (some of which show normal fault mechanisms) that approximately follows the 14°40′N cross-chain, and this could be associated with extension. If the 14°40′N zone has been extensional for the last few Ma, this would have allowed adiabatic decompression to form Chaife magmas.

Eruption of compositionally similar ankaramite several hundred thousand years after the picrite indicates that the production of high-MgO lavas was not an isolated event. Furthermore, it suggests that primitive lavas may have been erupted from other seamounts in the cross-chain. The greater normative Di and Ni contents, lower Ce contents and slightly different Pb isotopic characteristics and ages suggest that the ankaramite arose from a separate melt in a similar source region.

Intriguingly, the bulk compositions, modeled parental magmas and MI compositions are only slightly less magnesian than the Archean komatiites (Fig. 4). This provides some support for models of komatiite petrogenesis in the Archean convergent margin environments. Grove and Parman (2004) noted that subduction zones could produce a range of magmas from boninite to komatiite during subduction initiation. It is possible that rifting of a mature arc could produce similar magmatism. However, we have not yet observed the range of magma types and the hydrous magmas expected with the process described by Grove and Parman. While the Chaife data may have ramifications for understanding the origins of the Archean komatiite, it is outside the scope of this paper to speculate further.

Conclusions

Lavas from the Chaife seamount have characteristics consistent with presumed primary magma compositions, i.e. Mg# > 70, Ni > 200 ppm and Cr > 400 ppm. The trace element patterns and isotopic compositions indicate that Chaife lavas are arc-like, but are relatively anhydrous melts that originated in an Indian mantle domain that typically produces more hydrous and fractionated Mariana arc melts.

Major element, trace element and volatile measurements of MIs in olivine phenocrysts support this contention. The MI data provide evidence for a parental magma with median contents of ~17.5% MgO and LILE, U and Na concentrations within the lowermost range of typical island arc tholeiites. We propose that these melts were derived from the decompression melting of metasomatized mantle. Evidence for decompression melts is provided by the high-MgO contents, low water contents and the subdued arc-like trace element patterns in the MI. The high-Fo olivine, high-Mg# CPX and magnesian MI compositions, coupled with the high degrees of melting and median temperature estimates (1,367°C at 1.0–1.5 GPa) for the generation of Chaife melts, indicate that these magmas originated near the core of the mantle wedge and not at the slab–wedge interface.

These data almost require that an unusual tectonic regime in the underlying mantle led to mantle upwelling. A potential cause for this is cross-chain normal faulting, which could in turn be due to a tear or some other discontinuity in the subducting plate.

References

Arai S (1994) Compositional variation of olivine–chromian spinel in Mg-rich magmas as a guide to their residual spinel peridotites. J Volcanol Geotherm Res 59:279–293

Bacon CR, Bruggman PE, Christiansen RL, Clynne MA, Donnelly-Nolan JM, Hildreth W (1997) Primitive magmas at five Cascade volcanic fields: melts from hot, heterogeneous sub-arc mantle. Can Mineral 35:397–423

Bacon CR, Newman S, Stolper (1992) Water, CO_2, Cl, and F in melt inclusions in phenocrysts from three holocene explosive eruptions, Crater Lake, Oregon E M. Am Mineral 77:1021–1030

Baker PE, Condliffe EJ (1996) Compositional variations in submarine volcanic ashes from the vicinity of the Vanuatu island arc; a response to ridge-arc collision? J Volcanol Geotherm Res 72:225–238

Ballhaus CG, Berry RF, Green DH (1991) High pressure calibration of the olivine–orthopyroxene-spinel oxygen barometer, implications for the oxidation sate of the upper mantle. Contrib Mineral Petrol 107:27–40

Barnes SJ, Roeder PL (2001) The range of spinel compositions in terrestrial mafic and ultramafic rocks. J Petrol 42:2279–2302

Bartels KS, Kinzler RJ, Grove TL (1994) High-pressure phase relations of primitive high-alumina basalts from Medicine Lake volcano, northern California. Contrib Mineral Petrol 108:253–270

Beattie P (1994) Systematics and energetics of trace-element partitioning between olivine and silicate melts; implications for the nature of mineral/melt partitioning. Chem Geol 117:57–71

Bloomer SH, Hawkins JW (1987) Petrology and geochemistry of boninite series volcanic rocks from the Mariana trench. Contrib Mineral Petrol 97:361–377

Bloomer SH, Stern RJ (2001) Mantle inputs to the subduction factory: detailed studies of the Southern Mariana Seamount Province, Eos Trans. AGU 82

Bloomer SH, Stern RJ, Smoot NC (1989) Physical volcanology of the submarine Mariana and volcano arcs. Bull Volcanol 51:210–224

Bryant CJ, Arculus RJ, Eggins SM (2002) The geochemical evolution of the Izu-Bonin system: a perspective from tephras recovered by deep-sea drilling. Geochem Geophys Geosys 4, doi:10.1029/2002GC000427

Cameron BI, Walker JA, Carr MJ, Patino LC, Matias O, Feigenson MD (2002) Flux versus decompression melting at stratovolcanoes in southeastern Guatemala. J Volcanol Geotherm Res 119:21–50

Class C, Miller DM, Goldstein SL, Langmuir CH (2000) Distinguishing melt and fluid subduction components in Unmak Volcanics, Aleutian Arc. Geochem Geophys Geosys 2, doi:10.1029/1999GC000010

Crawford AJ, Falloo TJ, Green DH (1989) Classification, petrogenesis and tectonic setting of boninites. In: Crawford AJ (ed) Boninites and related rocks. Unwin Hyman, London, pp 1–48

Danyushevsky LV (2001) The effect of small amounts of H_2O on crystallisation of mid-ocean ridge and backarc basin magmas. J Volcanol Geotherm Res 110:265–280

Danyushevsky LV, Falloon TJ, Sobolev AV, Crawford AJ, Carroll M, Price RC (1993) The H_2O content of basalt glasses from southwest Pacific back-arc basins. Earth Planet Sci Lett 117:347–362

Danyushevsky LV, Sobolev AV, Falloon TJ (1995) North Tongan high-Ca boninite petrogenesis: the role of Samoan plume and subduction-transform fault transition. J Geodyn 20:219–241

Danyushevsky LV, Della-Pasqua FN, Sokolov S (2000) Reequilibration of melt inclusions trapped by magnesian olivine phenocryts from subduction-related magmas: petrological implications. Contrib Mineral Petrol 138:68–83

Danyushevsky LV, McNeill AW, Sobolev AV (2002) Experimental and petrological studies of melt inclusions in phenocrysts from mantle-derived magmas: an overview of techniques, advantages and complications. Chem Geol 183:5–24

Davies JH, Stevenson DJ (1992) Physical models of source region of subduction zone volcanics. J Geophys Res 97:2037–2070

Davidson JP (1996) Deciphering mantle and crustal signatures in subduction zone magmatism. In: Bebout GE, Scholl DW, Kirby SH, Platt JP (eds) Subduction top to bottom. American Geophysical Union, Washington, pp 251–262

Della-Pasqua FN, Varne R (1997) Primitive ankaramitic magmas in volcanic arcs: a melt inclusion approach. Can Mineral 35:291–312

Dick HJB (1989) Abyssal peridotites, very slow spreading ridges and ocean ridge magmatism. In: Saunders AD, Norry MJ (eds) Magmatism in the ocean basins. Geo Soc Special Pub 42:71–105

Dick HJB, Bullen T (1984) Chromian spinel as a petrogenetic indicator in abyssal and alpine-type peridotites and spatially associated lavas. Contrib Mineral Petrol 86:54–76

Dick HJB, Fisher RL (1983) Mineralogic studies of the residues of mantle melting: Abyssal and alpine type peridotites. In: Kornprobst J (eds) Kimberlites II: the mantle and crust-mantle relationships. Elsevier, New York pp 295–308

Dixon TH, Stern RJ (1983) Petrology, chemistry, and isotopic composition of submarine volcanoes in the southern Mariana arc. GSA Bull 94:1159–1172

Dobson PF, Skosby H, Rossman GR (1995) Water in boninite glass and coexisting orthopyroxene: concentration and partitioning. Contrib Mineral Petrol 118:414–419

Donaldson CH (1976) An experimental investigation of olivine morphology. Contrib Mineral Petrol 57:187–213

Draper DS, Johnston AD (1992) Anhydrous *P–T* phase relations of an Aleutian high-MgO basalt: an investigation of the role of olivine-liquid reaction in the generation of arc high-alumina basalts. Contrib Mineral Petrol 112:501–519

Eggins SM (1993) Origins and differentiation of picritic arc magmas, Ambae (Aoba), Vanuatu. Contrib Mineral Petrol 114:79–100

Elliot T, Plank T, Zindler A, White W, Bourdon B (1997) Element transport from slab to volcanic front at the Mariana arc. J Petrol 41:229–256

Elthon D, Stewart M, Ross DK (1992) Compositional trends of minerals in oceanic cumulates. J Geophys Res B 97:15189–15199

Fabriés J (1979) Spinel-olivine geothermometry in peridotites from ultramafic complexes. Contrib Mineral Petrol 69:329–336

Falloon TJ, Danyushevsky LV (2000) Melting of refractory mantle at 1.5, 2 and 2.5 GPa under anhydrous and H2O-saturated conditions: implications for the petrogenesis of high-Ca boninites and the influence of subduction components on mantle melting. J Petrol 41:257–283

Falloon TJ, Danyushevsky LV, Green DH (2001) Peridotite melting at 1 GPa: reversal experiments on partial melt compositions produced by peridotite-basalt sandwich experiments. J Petrol 42:2636–2390

Faure F, Schiano P (2005) Experimental investigation of equilibration conditions during forsterite growth and melt inclusion formation. Earth Planet Sci Lett 236:882–898

Faure F, Trolliard G, Nicollet C, Montel J-M (2003) A developmental model of olivine morphology as a function of the cooling rate and the degree of undercooling. Contrib Mineral Petrol 145:251–263

Foden JD, Green DH (1992) Possible role of amphibole in the origin of andesite; some experimental and natural evidence. Contrib Mineral Petrol 109:479–493

Ford CE, Russell DG, Craven JA, Fisk MR (1983) Olivine-liquid equilibria: temperature, pressure and compositional dependence of the crystal/liquid cation partition coefficient. J Petrol 24:256–265

Forsythe LM, Nielsen RL, Fisk MR (1992) High field-strength element partitioning between pyroxene and basaltic to dacitic magmas. Chem Geol 117:107–125

Fram MS, Longhi J (1992) Phase equilibria of dikes associated with Proterozoic anorthite complexes. Am Mineral 77:117–136

Fujimaki H, Tatsumoto M (1984) Partition coefficients of Hf, Zr and REE between phenocrysts and groundmass. J Geophys Res 89:662–672

Furukawa Y (1993) Magmatic processes under arcs and formation of the volcanic front. J Geophys Res 98:8309–8319

Gaetani GA, Watson EB (2002) Modeling the major-element evolution of olivine hosted melt inclusions. Chem Geol 183:25–41

Gaetani GA, Watson EB (2000) Open system behavior of olivine-hosted melt inclusions. Earth Planet Sci Lett 183:27–41

Gaetani G, Grove T (1998) The influence of water on the melting of mantle peridotite. Contrib Mineral Petrol 131:323–346

Gaetani G, Grove T (2003) Experimental constraints on melt generation. In: Eiler J (eds) Inside the subduction factory, Geophysical Monograph 138, American Geophysical Union, pp 107–134

Gaetani G, Grove GA, Bryan TL, Wilfred B (1993) The influence of water on the petrogenesis of subduction-related igneous rocks. Nature 365:332–334

Gill JB (1981) Orogenic andesite and plate tectonics. Springer, Berlin Heidelberg New York

Green DH, Schmidt MW, Hibberson WO (2004) Island-arc ankaramites: primitive melts from fluxed refractory lherzolitic mantle. J Petrol 45:391–403

Gribble Stern, Bloomer S, Stuben, O'Hearn, Newman (1996) MORB mantle and subduction components interact to generate basalts in the southern Mariana Trough back-arc basin. Geochim Cosmochim Acta 60:2153–2166

Grove TL, Kinzler RJ, Bryan WB (1992) Fractionation of mid-ocean ridge basalt (MORB). In: Mantle flow and melt generation at mid-ocean ridges. Geophys Mongr 71:281–310

Grove TL, Parman SW (2004) Thermal evolution of the Earth as recorded by komatiites. Earth Planet Sci Lett 219:173–187

Gust DA, Perfit MR (1987) Phase relations of a high-Mg basalt from the Aleutian island arc: implications for primary island arc basalts and high-Al basalts. Contrib Mineral Petrol 97:7–18

Gvirtzman Z, Nur A (1999) The formation of Mount Etna as the consequence of slab rollback. Nature 401:782–785

Hall PS, Kincaid C (2001) Diapiric flow at subduction zones: a recipe for rapid transport. Nature 292:2472–2475

Hart SR (1984) A large scale isotope anomaly in the Southern Hemisphere mantle. Nature 309:753–757

Hawkesworth CJ, Turner SP, McDermott F, Peate DW, von Calstern P (1997) U–Th isotopes in arc magmas: implications for element transfer from subducted crust. Science 276:551–555

Hawkins J (2003) High-Mg rocks of a Tonga (Tofua) arc seamount: implications for early arc history. In: Geological Society of America annual meeting, GSA Abstracts with Programs 35

Hirschmann M, Wiens D, Peacock S (2000) Subduction Factory Science Plan: NSF Margins Initiative. http://www.ldeo.columbia.edu/margins/SF_Sci_Plan_revised.pdf, 42 p

Jacques AL, Green DH (1980) Anhydrous melting of peridotite at 0–15 kbar pressure and the generation of tholeiitic basalts. Contrib Mineral Petrol 73:287–310

Johnson MC, Plank T (1999) Dehydration and melting experiments constrain the fate of subducted sediments. Geochem Geophys Geosys 1, 1999GC000014

Johnston AD, Draper DS (1992) Near-liquidus phase relations of an anhydrous high-magnesia basalt from the Aleutian Islands: Implications for arc magma genesis and ascent. J Volcanol Geotherm Res 52:27–41

Kamenetsky VS, Metrich N, Cioni R (1995) Potassic primary melts of Vulsini (Roman Province): evidence from mineralogy and melt inclusions. Contrib Mineral Petrol 120:186–196

Kamenetsky VS, Crawford AJ, Meffre S (2001) Factors controlling chemistry of magmatic spinel: an empirical study of associated olivine, Cr-spinel and melt inclusions from primitive rocks. J Petrol 42:655–671

Kennedy AK, Lofgren GE, Wasserburg GJ (1993) An experimental study of trace element partitioning between olivine, orthopyroxene and melt in chondrules: equilibrium values and kinetic effects. Earth Planet Sci Lett 219(115):177–195

Kent AJR, Elliot TR (2002) Melt inclusions from Marianas arc lavas: implications for the composition and formation of island arc magmas. Chem Geol 183:263–286

Kent AJR, Stolper EM, Francis D, Woodhead J, Frei R, Eiler J (2004) Mantle heterogeneity during the formation of the North Atlantic Tertiary Province: constraints from trace element and Sr–Nd–Os–O isotope systematics of Baffin Island picrites. Geochem Geophys Geosyst 5: Q11004, doi: 10.1029/2004GC000743

Kimura J-I, Stern RJ, Yoshida T (2005) Reinitiation of subduction and magmatic responses in SW Japan during Neogene time. GSA Bull 117:969–986

Kohut EJ, Nielsen RL (2004) Melt inclusion formation mechanisms and compositional effects in high-An feldspar and high-Fo olivine in anhydrous mafic silicate liquids. Contrib Mineral Petrol 147(6):684–704

Leat PT, Larter RD (2003) Intra-oceanic subduction systems: introduction. Geol Soc Lond Spec Pub 219:1–17

Le Bas MJ (2000) IUGS reclassification of the high-Mg and picrite volcanic rocks. J Petrol 41:1467–1470

Lee J, Stern RJ (1998) Glass inclusions in Mariana arc phenocrysts; a new perspective on magmatic evolution in a typical intra-oceanic arc. J Geol 106:19–33

Lofgren G (1974) An experimental study of plagioclase crystal morphology: isothermal crystallization. Am J Sci 274:243–273

Manton WI (1988) Separation of Pb from young zircons by single-bead ion exchange. Chem Geol 73:147–152

McDonough WF, Sun SS (1995) The composition of the Earth. Chem Geol 120:223–253

Miller MS, Gorbatov A, Kennett BL, Stern RJ, Gvirtzman Z (2004) Tear in the subducting slab beneath the Southern Mariana Arc: evidence from P-wave Tomography. Eos Trans AGU 85

Monzier M, Robin C, Eissen J-P, Cotton J (1997) Geochemistry vs. seismo-tectonics along the New Hebrides Central Chain (Southwest Pacific). J Volcanol Geotherm Res 78:1–29

Myers JD, Johnston AD (1996) Phase equilibria constraints on subduction zone magmatism. In: Bebout GE, Scholl DW, Kirby SH, Platt JP (eds) Subduction top to bottom. American Geophysical Union, Washington, 229–250

Newman S, Stolper E, Stern RJ (2000) H_2O and CO_2 in magmas from the Mariana arc and back arc systems. Geochem Geophys Geosys 1, 1999GC000027

Nielsen RL, Crum J, Bourgeois R, Hascall K, Forsythe LM, Fisk MR, Christie DM (1995) Melt inclusions in high-An plagioclase from the Gorda Ridge, an example of the local diversity of MORB parent magmas. Contrib Mineral Petrol 122:34–50

Nielsen RL, Peter MJ, Sours-Page R (1998) Chemical and physical indicators of compromised melt inclusions. Geochim Cosmochim Acta 62:831–839

Nye CJ, Reid MR (1986) Geochemistry of primary and least fractionated lavas from Okmok volcano, central Aleutians: implications for arc magmagenesis. J Geophys Res 91:10271–10287

Osborn EF, Tait DB (1952) The system diopside–anorthite–forsterite. Am J Sci Bowen volume 413–433

Peacock SM (2003) Thermal and metamorphic evolution of subducting slabs. In: Eiler (ed) Inside the subduction factory. Geophys Monogr 138, AGU 7–22

Peacock SM, Wang K (1999) Seismic consequences of warm versus cool subduction metamorphism; examples from Southwest and Northeast Japan. Science 286:937–939

Pearce JA, Peate DW (1995) Tectonic implications of the compositions of volcanic arc magmas. Annu Rev Earth Planet Sci 23:251–285

Pearce JA, Kempton PD, Nowell GM, Noble SR (1999) Hf–Nd element and isotope perspectives on the nature and provenance of mantle and subduction components in Western Pacific arc-basin systems. J Petrol 40:1579–1611

Pearce JA, Parkinson IJ (1993) Trace element models for mantle melting: application to volcanic arc petrogenesis. In: Pritchard HM, Alabaster T, Narris NBW, Neary CR (eds) Magmatic processes and plate tectonics. Geological Society Special Pub 76:373–403

Peate DW, Pearce JA, Hawkesworth CJ, Colley H, Edwards CMH, Hirose K (1997) Geochemical variations in Vanuatu arc lavas: the role of subducted material and a Variable mantle wedge composition. J Petrol 38:1331–1358

Plank T, Langmuir CH (1998) The chemical composition of subducting sediment and its consequences for the crust and mantle. Chem Geol 145:325–394

Presnall DC, Dixon SA, Dixon JR, O'Donnell TH, Brenner NL, Schrock RL, Ducus DW (1978) Liquidus phase relations on the join diopside-forsterite-anorthite from 1 atm to 20 kbar: their bearing on the generation and crystallization of basaltic magma. Contrib Mineral Petrol 66:203–220

Putirka K, Johnson M, Kinzler R, Longhi R, Walker D (1996) Thermobarometry of mafic igneous rocks based on clinopyroxene-liquid equilibria, 0–30 kbar. Contrib Mineral Petrol 123:92–108

Putirka KD, Mikaelian H, Ryerson F, Shaw H (2003) New clinopyroxene-liquid thermobarometers for mafic, evolved, and volatile-bearing lava composition, with applications to lavas from Tibet and the Snake River plain, Idaho. Am Mineral 88:1542–1554

Ramsay WRH, Crawford AJ, Foden JD (1984) Field setting, mineralogy, chemistry and genesis of arc picrites, New Georgia, Solomon Islands. Contrib Mineral Petrol 88:386–402

Roeder PL, Emslie RF (1970) Olivine-liquid equilibrium. Contrib Mineral Petrol 29:275–289

Roeder PL, Campbell JH, Jamieson HE (1979) A re-evaluation of the olivine-spinel geothermometer. Contrib Mineral Petrol 68:325–334

Roedder E (1979) Origin and significance of magmatic inclusions. Bull Mineral 102:487–510

Roedder E (1984) Fluid inclusions. In: Ribbe PH (ed) Reviews in mineralogy, vol 12. Mineralogical Society of America, Blacksburg, 646 p

Rohrbach A, Schuth S, Ballhaus C, MünkerC, Mateev S, QopotoC (2005) Petrological constraints on the origins of arc picrites, New Georgia Group, Solomon Islands. Contrib Mineral Petrol 149:685–698

Saal AE, Hart SR, Shimizu N, Hauri EH, Layne GD (1998) Pb isotopic variability in melt inclusions from oceanic island basalts, Polynesia. Science 282:1481–1484

Sakuyama M (1979) Lateral variation of H_2O contents in Quaternary magmas of north-eastern Japan. Earth Planet Sci Lett 43:103–111

Scott DR, Stevenson DJ (1986) Magma ascent by porous flow. J Geophys Res 91:9238–9296

Scowen PAH, Roeder PL, Helz RT (1991) Reequilibration of of chromite within Kilauea Iki lava lake, Hawaii. Contrib Mineral Petrol 107:8–20

Scuth S, Ronrbach A, Münker C, Ballhaus S (2003) Petrogenesis of arc picrites and basalts from the New Georgia group, Solomon Islands-a geochemical approach. Geophysical Research Abstracts 5, 06541

Schwab BE, Johnston AD (2001) Melting sytematics of modally variable, compositionally intermediate peridotites and the effects of mineral fertility. J Petrol 42:1789–1811

Schwandt C, McKay G (1998) Rare, Earth element partition coefficients from enstatite/melt synthesis experiments. Geochim Cosmochim Acta 62(16):2845–2848

Shimizu H, Sangen K, Masuda A (1982) Experimental study on rare-Earth element partitioning in minerals formed at 10 and 20 kbar for basaltic systems. Geochem J 16:107–117

Simkin T, Smith JV (1970) Minor-element distribution in olivine. J Geol 78:304–325

Sisson TW, Bronto S (1998) Evidence for pressure-release melting beneath magmatic arcs from basalt at Galunggung, Indonesia. Nature 391:883–886

Sisson TW, Layne GD (1993) H$_2$O in basalt and basaltic andesite glass inclusions from four subduction related volcanoes. Earth Planet Sci Lett 117:619–635

Sobolev AV (1996) Melt inclusions in minerals as a source of petrological information. Petrologia 4:228–239

Sobolev AV, Danyushevsky LV (1994) Petrology and geochemistry of boninites from the north termination of the Tonga Trench: constraints on the generation conditions of primary high-Ca boninite magmas. J Petrol 35:1183–1211

Sours-Page R, Johnson KTM, Nielsen RL, Karsten JL (1999) Local and regional variation of MORB parent magmas: evidence from melt inclusions from the Endeavour segment of the Juan de Fuca Ridge. Contrib Mineral Petrol 134:342–363

Stern RJ (2002) Subduction zones. Rev Geophys doi:10.1029/2001RG000108

Stern RJ, Bibee LD (1984) Esmeralda Bank: geochemistry of a submarine volcano in the Mariana Island arc. Contrib Mineral Petrol 86:159–169

Stern RJ, Fouch MJ, Klemperer SL (2003) An overview of the Izu-Bonin-Mariana subduction factory. In: Eiler J (eds) Inside the subduction factory. Geophysical Monograph 138, American Geophysical Union, doi: 10.1029/138GM10

Takahashi E (1978) Partioning of Ni^{2+}, Co^{2+}, Fe^{2+}, Mn^{2+} and Mg^{2+} between olivine and silicate melts-compositional dependence of partition coefficients. Geochim Cosmochim Acta 42:1829–1844

Tamura Y, Tatsumi Y, Zhao D, Kidoa Y (2002) Hot fingers in the mantle wedge: new insights into magma genesis in subduction zones. Earth Planet Sci Lett 197:105–116

Tatsumi Y (1982) Origin of high-magnesian andseites in the Setouchi volcanic belt, southwest Japan, II: melting experiments at high pressures. Earth Planet Sci Lett 60:305–317

Tatsumi Y, Eggins S (1995) Subduction zone magmatism. Blackwell, Cambridge

Tatsumi Y, Furukawa Y, Yamashita S (1994) Thermal and geochemical evolution of the mantle wedge in the NE Japan arc I: contribution from experimental petrology. J Geophys Res 99:22275–22283

Tatsumi Y, Sakuyama M, Fukuyama H, Kushiro I (1983) Generation of arc basalt magmas and thermal structure of the mantle wedge in subduction zones. J Geophys Res B 88:5815–5825

Tatsumi Y, Shukuno H, Sato K, Shibata T, Yshikawa M (2003) The petrology and geochemistry of high-magnesium andesites at the western tip of the Setouchi Volcanic Belt, SW Japan. J Petrol 44:1561–1578

Taylor SR, Mclennan SM (1995) The geochemical evolution of the continental crust. Rev Geophys 33:241–265

van Keken PE, Kiefer B, Peacock SM (2002) High-resolution models of subduction zones: implications for mineral dehydration reactions and the transport of water into the deep mantle. Geochem Geophys Geosys 3, doi:10.1029/2001GC000256

Wallace PJ (2002) Volatiles in submarine basaltic glasses from the Northern Kerguelen Plateau (ODP Site 1140): implications for source regions compositions, magmatic processes, and plateau subsidence. J Petrol 43:1311–1326

Yamakazi T, Stern RJ (1997) Topography and magnetic vector anomalies in the Mariana Trough. JAMSTEC J Deep Sea Res 13:31–45

Yoder HS, Tilley CE (1962) Origin of basalt magmas: and experimental study of natural and synthetic rock systems. J Petrol 3:342–532